


Phenomenology of a Born-Infeld extension of the $U(1)_Y$ sector at lepton colliders

P. De Fabritiis^{1,*}, P. C. Malta^{2,†} and J. A. Helayël-Neto^{1,‡}

¹*Centro Brasileiro de Pesquisas Físicas (CBPF),
Rua Dr Xavier Sigaud 150, Urca, Rio de Janeiro, Brazil, 22290-180*

²*R. Antonio Vieira 23, 22010-100, Rio de Janeiro, Brazil*

 (Received 24 September 2021; accepted 22 December 2021; published 7 January 2022)

In this work, we perform a nonlinear extension of the $U(1)_Y$ sector of the Standard Model leading to novel quartic effective interactions between the neutral gauge bosons. We study the induced effects through high-energy processes resulting in three photons, namely, Z-boson decay and electron-positron annihilation. Available experimental data on these processes do not yield viable lower bounds on the mass parameter $\sqrt{\beta}$, but we estimate that the range $\sqrt{\beta} \lesssim m_Z$ could be reliably excluded with better statistics in future e^-e^+ colliders. We also discuss neutral gauge-boson scatterings, contextualizing our findings with recent results on anomalous quartic gauge couplings.

DOI: [10.1103/PhysRevD.105.016007](https://doi.org/10.1103/PhysRevD.105.016007)

I. INTRODUCTION

The idea of nonlinear electromagnetic responses of the vacuum was first suggested by Halpern [1] and one year later by Heisenberg [2], where he proposed that virtual electron-positron pairs could be at the origin of photon-photon collisions. Soon thereafter, actions with nonlinear electrodynamics were introduced by Born and Infeld [3] and also Euler and Heisenberg [4] in the 1930s to deal with the classical problem of the infinite self-energy of a point charge. These extensions, which have been also explored in areas as diverse as black-hole physics and cosmology [5–8], can display interesting features, such as vacuum birefringence and dichroism [9–11]. For recent developments, see Refs. [12–14] and references therein.

Perhaps the most striking prediction of these models is the occurrence of light-by-light scattering already at tree level. This extremely rare process was recently observed by the ATLAS and CMS collaborations in heavy-ion collisions at the LHC [15–17]. The perspective to test effects of nonlinear extensions of the Standard Model (SM) in high-energy experiments—in lepton and hadron accelerators or potentially in photon colliders—motivates us to search for possible phenomenological consequences.

The nonlinear extension of traditional Maxwell electrodynamics modifies photon-photon interactions by introducing higher-order terms in the Lagrangian. Here, we are interested in extending the whole hypercharge sector of the electroweak gauge group, thus giving rise to other interesting phenomena. In fact, besides reproducing the already known nonlinear effects in standard electrodynamics (corrected by a factor involving the Weinberg angle), this extension induces anomalous quartic couplings between the Z-boson and the photon. This in turn theoretically allows for rare processes to take place already at tree level, as for example the creation of a Z-boson pair from the collision of two photons.

There is also a more recent motivation for considering nonlinear models. Introduced by Dirac 90 years ago [18], magnetic monopoles remain elusive, despite experimental efforts. It was thought for a long time that it would be impossible to obtain a monopole solution in the electroweak sector because of its gauge structure after symmetry breaking, but this belief turned out to be wrong. An electroweak monopole solution was obtained by Cho and Maison [19], but the original solution predicted an infinite mass that should be regularized to have physical meaning and sustain any hope of being found experimentally. A few years ago, some proposals of SM extensions regularizing the monopole energy and giving a finite, calculable mass were made [20–22]. A nonlinear extension of the hypercharge sector could solve the infinite-energy problem [23]; a more general extension of the $U(1)_Y$ sector giving a finite-energy monopole solution was investigated in Ref. [24]. Nowadays, there is hope to finally find a monopole in dedicated experiments, such as MoEDAL at

*pdf321@cbpf.br
†pedrocmalta@gmail.com
‡helayel@cbpf.br

Published by the American Physical Society under the terms of the [Creative Commons Attribution 4.0 International license](https://creativecommons.org/licenses/by/4.0/). Further distribution of this work must maintain attribution to the author(s) and the published article's title, journal citation, and DOI. Funded by SCOAP³.

CERN [25], so it is imperative to understand the phenomenological implications of such an extension.

Nonlinear effects have not been observed at low energies. This means that the parameter controlling the nonlinearity of the fields is expected to be large in comparison to other relevant energy scales. The parameters in nonlinear theories may be constrained in different ways, e.g., via hydrogen spectroscopy or interferometry [26,27]. A more stringent bound is obtained using LHC data on light-by-light scattering in heavy-ion collisions [28]. The lower bound reported there is ~ 100 GeV, but it could reach ~ 200 GeV under less restrictive assumptions. The ATLAS data on $gg \rightarrow \gamma\gamma$ can enhance this sensitivity by 1 order of magnitude in a Born-Infeld (BI) extension of SM [29], reaching the TeV scale as in brane-inspired models.

In this work, we analyze an extension of the hypercharge sector of the SM. This gives rise to quartic effective interactions between the neutral gauge bosons absent in the SM at tree level. These novel operators contribute to decay and scattering processes, and we explore existing experimental data to place lower bounds on the nonlinear parameter. We discuss recent results constraining anomalous gauge couplings and briefly consider possible improvements on these bounds in future experiments.

This paper is organized as follows. In Sec. II, we present the theoretical setup of our model. In Sec. III, we discuss options to constrain the expansion parameter β , in particular through the decay $Z \rightarrow 3\gamma$ in Sec. III A and the scattering $e^-e^+ \rightarrow 3\gamma$ in Sec. III B. In Sec. III C, we discuss neutral gauge-boson scattering processes and contextualize our discussion with recent results in anomalous quartic gauge couplings. Finally, in Sec. IV, we present our closing remarks. We use natural units ($c = \hbar = 1$) and the flat Minkowski metric $\eta^{\mu\nu} = \text{diag}(+1, -1, -1, -1)$ throughout.

II. THEORETICAL SETUP

Let us briefly review the usual electroweak (EW) Lagrangian to fix our notation. The bosonic part of the EW sector is given by

$$\mathcal{L}_{\text{EW}} = \mathcal{L}_{\text{Gauge}} + \mathcal{L}_{\text{Higgs}}, \quad (1)$$

where

$$\mathcal{L}_{\text{Gauge}} = -\frac{1}{4} F_{\mu\nu}^a F_{\mu\nu}^a - \frac{1}{4} B_{\mu\nu} B_{\mu\nu}, \quad (2)$$

$$\mathcal{L}_{\text{Higgs}} = |D_\mu H|^2 - \lambda \left(H^\dagger H - \frac{m^2}{2\lambda} \right)^2. \quad (3)$$

Here, we defined the covariant derivative as

$$D_\mu = \partial_\mu - igA_\mu^a T^a - ig' Y B_\mu. \quad (4)$$

In the equations above, A_μ^a and B_μ are the gauge fields associated with the gauge group $SU(2)_L \times U(1)_Y$, $F_{\mu\nu}^a = \partial_\mu A_\nu^a - \partial_\nu A_\mu^a + g\epsilon_{abc} A_\mu^b A_\nu^c$ and $B_{\mu\nu} = \partial_\mu B_\nu - \partial_\nu B_\mu$ are the respective field strengths, and g and g' are the couplings. Here, T^a are the generators of $SU(2)_L$ satisfying $[T^a, T^b] = i\epsilon^{abc} T^c$, and Y is the weak hypercharge.

The Higgs field H is a $SU(2)_L$ doublet with hypercharge $Y(H) = +1/2$. The scalar potential induces a nontrivial vacuum expectation value given by $|\langle H \rangle|^2 = v^2/2 = m^2/2\lambda$. Below this energy scale, the theory is cast into the Higgs phase with three massive vector bosons W^\pm, Z , a massive scalar h and a massless photon A (γ) in the spectrum. The physical fields can be written using the Weinberg angle θ_W : the neutral vector bosons are defined by $Z_\mu = \cos\theta_W A_\mu^3 - \sin\theta_W B_\mu$ and $A_\mu = \sin\theta_W A_\mu^3 + \cos\theta_W B_\mu$, whereas the charged vector fields are defined by $W_\mu^\pm = (A_\mu^1 \mp iA_\mu^2)/\sqrt{2}$.

The masses of the vector bosons can be precisely measured and are $m_W = gv/2 = 80.4$ GeV and $m_Z = m_W/\cos\theta_W = 91.2$ GeV. The Weinberg angle can be experimentally determined and satisfies $\sin^2\theta_W = 0.23$. After symmetry breaking, the kinetic part of the gauge Lagrangian (omitting mass terms) reads

$$\mathcal{L}_{\text{Gauge}}^{\text{Kin}} = -\frac{1}{4} F_{\mu\nu} F^{\mu\nu} - \frac{1}{4} Z_{\mu\nu} Z^{\mu\nu} - \frac{1}{2} W_{\mu\nu}^+ W^{\mu\nu-}, \quad (5)$$

where the field-strength tensors are defined as usual.

We may now introduce the leptons through the following Lagrangian,

$$\mathcal{L}_{\text{Leptons}} = i\bar{L}_i \gamma^\mu D_\mu L_i + i\bar{\ell}_{iR} \gamma^\mu D_\mu \ell_{iR}, \quad (6)$$

where L_i denotes the lepton doublets $L_i = (\nu_{iL} \ell_{iL})^t$ with ν_{iL} , ℓ_{iL} , and ℓ_{iR} representing the left-handed neutrinos, the left-handed charged leptons, and the right-handed lepton fields, respectively. Here, i is a flavor index to distinguish between the three generations of leptons. The hypercharge assignment adopted here is $Y(L_i) = -1/2$ and $Y(\ell_{iR}) = -1$. Taking Eq. (6) with Eq. (4), including the gauge fields after symmetry breaking, we obtain the interactions between matter and gauge fields. In what follows, only two such interaction terms will be relevant, namely,

$$\mathcal{L}_{ee\gamma} = -e\bar{\ell}_i \gamma_\mu \ell_i A^\mu, \quad (7)$$

$$\mathcal{L}_{eeZ} = \frac{g}{4\cos\theta_W} \bar{\ell}_i \gamma_\mu (-1 + 4\sin^2\theta_W + \gamma^5) \ell_i Z^\mu. \quad (8)$$

Here, we propose the following general extension of the weak hypercharge sector of the EW Lagrangian,

$$\mathcal{L} = -\frac{1}{4} B_{\mu\nu} B^{\mu\nu} \rightarrow \mathcal{L}_Y = f(\mathcal{F}, \mathcal{G}), \quad (9)$$

where we defined the Lorentz and gauge invariant objects

$$\mathcal{F} = \frac{1}{4} B_{\mu\nu} B^{\mu\nu} \quad \text{and} \quad \mathcal{G} = \frac{1}{4} B_{\mu\nu} \tilde{B}^{\mu\nu} \quad (10)$$

with the dual field-strength tensor given by $\tilde{B}^{\mu\nu} = \frac{1}{2} \epsilon^{\mu\nu\rho\sigma} B_{\rho\sigma}$. This type of nonlinear extension was already studied in the context of magnetic monopoles [24], where it was shown that under certain conditions it allows a finite-energy electroweak monopole solution.

The SM predictions are so far in excellent agreement with experiment, and in order to recover the usual SM results, we demand that our general extension $f(\mathcal{F}, \mathcal{G})$ reproduces the usual term $-\frac{1}{4} B_{\mu\nu} B^{\mu\nu}$ in some appropriate limit. Since we do not want to have a parity-violating term in the photon sector after spontaneous symmetry breaking, we impose the physically motivated assumption that $f(\mathcal{F}, \mathcal{G})$ depends on \mathcal{G} only through \mathcal{G}^2 .

Let us consider for instance a BI extension of the hypercharge sector [3] given by

$$\mathcal{L}_Y^{\text{BI}} = \beta^2 \left[1 - \sqrt{1 + 2 \left(\frac{\mathcal{F}}{\beta^2} - \frac{\mathcal{G}^2}{2\beta^4} \right)} \right], \quad (11)$$

where β is a parameter with dimension of mass squared. This nonlinear extension has been extensively studied in the context of electrodynamics, with applications in a range of subjects, and has attracted a lot of interest in recent years after the observation of light-by-light scattering at the LHC [15–17]. Interestingly enough, the BI action can be derived from string theory [30] and also appears in the dynamics of D-branes [31].

Our goal is to study the phenomenological consequences of the nonlinear extension in high-energy processes. To accomplish this, we need to obtain the induced operators

$$\begin{aligned} \mathcal{L}_Y^{(1/\beta^2)} = & \frac{1}{32\beta^2} \{ s_\theta^4 [(ZZ)(ZZ) + (Z\tilde{Z})(Z\tilde{Z})] + c_\theta^4 [(FF)(FF) + (F\tilde{F})(F\tilde{F})] + 2s_\theta^2 c_\theta^2 [(FF)(ZZ) + (F\tilde{F})(Z\tilde{Z})] \\ & + 4s_\theta^2 c_\theta^2 [(ZF)(ZF) + (Z\tilde{F})(Z\tilde{F})] - 4s_\theta^3 c_\theta [(ZZ)(ZF) + (Z\tilde{Z})(Z\tilde{F})] - 4s_\theta c_\theta^3 [(FF)(FZ) + (F\tilde{F})(F\tilde{Z})] \}, \quad (13) \end{aligned}$$

where we defined $(ZZ) \equiv Z_{\mu\nu} Z^{\mu\nu}$ with an analogous definition for the dual versions. All non-linearly induced vertices above have the same momentum structure and very similar Feynman rules; this traces back to the common origin of such interactions.

In conclusion, we see that our nonlinear extension in the hypercharge sector generates a series of dimension-8 effective operators generically suppressed by a factor $(\mathcal{E}/\Lambda)^4$, where \mathcal{E} is a typical energy scale characteristic

written in terms of the physical fields after symmetry breaking. The mass scale set by $\sqrt{\beta}$ is expected to be large in comparison with the typical energies of the processes considered, motivating us to perform a Taylor expansion of Eq. (11) in powers of $X = \frac{\mathcal{F}}{\beta^2} - \frac{\mathcal{G}^2}{2\beta^4}$:

$$\mathcal{L}_Y = -\mathcal{F} + \frac{1}{2\beta^2} [\mathcal{F}^2 + \mathcal{G}^2] + \mathcal{O}(1/\beta^4). \quad (12)$$

We will only consider tree-level processes with at most four gauge bosons in each vertex, so we can safely restrict ourselves to leading nontrivial order. It is important to keep in mind that this perturbative approach can only be trusted as long as the energy of the process is lower than the mass scale set by $\sqrt{\beta}$, as this guarantees that the next terms in the expansion provide increasingly negligible corrections to the leading-order terms.

Furthermore, taking into consideration the recent interest in different versions of nonlinear electrodynamics, we can also consider other interesting extensions that would give rise to the same physical effects in the approximation considered here. In fact, using X defined above, we could as well have considered here the extensions given by $\mathcal{L}_Y^{\text{Log}} = -\beta^2 \log[1 + X]$ and $\mathcal{L}_Y^{\text{Exp}} = \beta^2 [e^{-X} - 1]$ giving us the $U(1)_Y$ version of the logarithmic [9] and exponential [10,11] nonlinear electrodynamics. The three extensions agree up to leading nontrivial order, and we will restrict ourselves to tree-level processes with at most four gauge bosons interactions, so we may safely consider the β parameters as being equal with a good approximation and use Eq. (12) to describe their common effects.

The Lagrangian above is a function of the $U(1)_Y$ gauge field, B_μ , but after symmetry breaking, we can write it in terms of the physical fields, A_μ and Z_μ , retrieving the usual SM kinetic terms at zeroth order. At first order, we have ($s_\theta \equiv \sin \theta_W$, $c_\theta \equiv \cos \theta_W$)

of the process and Λ is the mass scale set by $\sqrt{\beta}$. These effective operators will introduce new vertices, allowing processes that could only occur in the SM at loop level to take place already at tree level. In the next section, we explore this fact and consider different high-energy processes to obtain lower bounds on β whenever experimental data are available. We also discuss the impact of our nonlinear extension on scattering processes involving neutral gauge bosons.

III. EXPERIMENTAL LIMITS

In the section above, we have extracted quartic interaction vertices between the photon and Z-boson which are completely absent from the SM, thus opening up interesting possibilities to constrain the expansion parameter β . In the following, we explore a few of them.

A. $Z \rightarrow 3\gamma$

In the SM, there is no tree-level $Z\gamma\gamma\gamma$ vertex, so the decay process $Z \rightarrow 3\gamma$ proceeds exclusively via fermion and W-boson loops [32,33]. The theoretical prediction for the partial width is $\Gamma(Z \rightarrow 3\gamma)_{\text{SM}} = 1.4 \text{ eV}$ [34], and given the experimentally determined total width of the Z-boson $\Gamma_{\text{exp}}^Z = 2.49 \text{ GeV}$ [35], the expected branching ratio is $\text{BR}(Z \rightarrow 3\gamma)_{\text{SM}} = 5.4 \times 10^{-10}$. The currently best upper bound was obtained by the ATLAS Collaboration using pp collisions at $\sqrt{s} = 8 \text{ TeV}$ and reads [36]

$$\text{BR}(Z \rightarrow 3\gamma)_{\text{exp}} < 2.2 \times 10^{-6}, \quad (14)$$

representing a fivefold improvement on the previous determination from LEP [37]. This process is clearly very rare and could not yet be measured directly. It is thus an ideal testing ground for new physics [38,39].

The SM prediction is compatible with the best current experimental bound, but there is a vast gap between them.

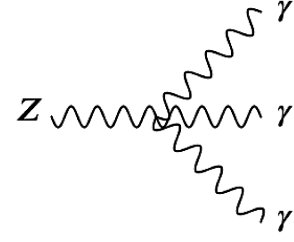


FIG. 1. Tree-level Feynman diagram for the decay $Z \rightarrow 3\gamma$.

The nonlinear extension can therefore be constrained by comparing its prediction to the experimental bound; cf. Eq. (14). The tree-level amplitude for a Z-boson with 4-momentum p decaying into three photons with 4-momenta q_k ($k = 1,2,3$) is (cf. Fig. 1)

$$-i\mathcal{M} = \epsilon_\alpha(p) V_{Z3\gamma}^{\alpha\beta\gamma\delta}(\beta) \epsilon_\beta^*(q_1) \epsilon_\gamma^*(q_2) \epsilon_\delta^*(q_3), \quad (15)$$

where the vertex factor

$$V_{Z3\gamma}^{\alpha\beta\gamma\delta}(\beta) = -i \frac{s_\theta c_\theta^3}{\beta^2} f^{\alpha\beta\gamma\delta} \quad (16)$$

may be read from the last line of Eq. (13). The momentum-dependent function $f^{\alpha\beta\gamma\delta}$ is given by

$$\begin{aligned} -f^{\alpha\beta\gamma\delta} = & [(q_1 \cdot q_2) \eta^{\beta\gamma} - q_1^\gamma q_2^\beta] [(p \cdot q_3) \eta^{\alpha\delta} - p^\delta q_3^\alpha] + [(q_1 \cdot q_3) \eta^{\beta\delta} - q_1^\delta q_3^\beta] [(p \cdot q_2) \eta^{\alpha\gamma} - p^\gamma q_2^\alpha] \\ & + [(q_2 \cdot q_3) \eta^{\gamma\delta} - q_2^\delta q_3^\gamma] [(p \cdot q_1) \eta^{\alpha\beta} - p^\beta q_1^\alpha] + \epsilon^{\mu\beta\gamma\gamma} \epsilon^{\nu\delta\kappa\alpha} p_\kappa q_{1\mu} q_{2\rho} q_{3\nu} \\ & + \epsilon^{\mu\beta\rho\delta} \epsilon^{\nu\gamma\kappa\alpha} p_\kappa q_{1\mu} q_{2\nu} q_{3\rho} + \epsilon^{\mu\gamma\rho\delta} \epsilon^{\nu\beta\kappa\alpha} p_\kappa q_{1\nu} q_{2\mu} q_{3\rho}. \end{aligned} \quad (17)$$

Here, we have assumed that p flows into the vertex, whereas the q_k flow out of it. Incidentally, this momentum structure is the same for all vertices in Eq. (13).

From this point on, we neglect the loop-level SM amplitude so the tree-level result from Eq. (15) is essentially the only contribution to the decay. The unpolarized squared amplitude reads

$$\langle |\mathcal{M}|^2 \rangle = \frac{8s_\theta^2 c_\theta^6}{3\beta^4} \Phi(p, q_1, q_2, q_3), \quad (18)$$

with the momentum factor given by

$$\Phi(p, q_1, q_2, q_3) = \frac{1}{2} (p \cdot q_1)^2 (q_2 \cdot q_3)^2 + \text{perm.}, \quad (19)$$

where ‘‘perm.’’ indicates all permutations of the q_k . In the rest frame of the decaying Z-boson, $p^\mu = (m_Z, 0)$, and the outgoing photons have $E_k = |\mathbf{q}_k|$. By applying the usual dispersion relations and momentum conservation, we find

$$p \cdot q_3 = m_Z E_3 \quad \text{and} \quad q_1 \cdot q_2 = \frac{m_Z^2}{2} - m_Z E_3, \quad (20)$$

with similar results for the other 4-momenta pairs. Therefore, we can rewrite $\Phi(p, q_1, q_2, q_3)$ as

$$\Phi(p, q_1, q_2, q_3) = \frac{m_Z^4}{4} \sum_{k=1,2,3} E_k^2 (m_Z - 2E_k)^2. \quad (21)$$

Notice that this expression is symmetric under the change of final photons, a reasonable behavior since there is no preferred photon in this decay. As the phase space integral also enjoys this symmetry, we can simply use one of the terms above to do the integration and multiply the output by 3, since they will necessarily give the same result. The partial width is defined as

$$d\Gamma = \frac{1}{3!} \frac{1}{2m_Z} \langle |\mathcal{M}|^2 \rangle d\Pi_3, \quad (22)$$

where $1/3!$ is the symmetry factor due to the identical photons in the final state. The three-body phase-space function is

$$d\Pi_3 = \frac{d^3\mathbf{q}_1}{(2\pi)^3 2E_1} \frac{d^3\mathbf{q}_2}{(2\pi)^3 2E_2} \frac{d^3\mathbf{q}_3}{(2\pi)^3 2E_3} \times (2\pi)^4 \delta^4(p - q_1 - q_2 - q_3). \quad (23)$$

We have then

$$d\Gamma = K \frac{E_3(m_Z - 2E_3)^2}{E_1 E_2} d^3\mathbf{q}_1 d^3\mathbf{q}_2 d^3\mathbf{q}_3 \times \delta^4(p - q_1 - q_2 - q_3), \quad (24)$$

where the constant K , already including the factor of 3, is

$$K = \frac{s_\theta^2 c_\theta^6 m_Z^3}{1536\pi^5 \beta^4}. \quad (25)$$

The rest of the calculation follows a path similar to the textbook calculation of muon decay [40]. The delta function may be split into two factors enforcing energy and 3-momentum conservation. The latter allows us to write $\mathbf{q}_2 \rightarrow -(\mathbf{q}_1 + \mathbf{q}_3)$ and $E_2 \rightarrow |\mathbf{q}_1 + \mathbf{q}_3|$. Let us take the polar axis along \mathbf{q}_3 , which is held fixed, so that

$$E_2(\cos\theta) = |\mathbf{q}_1 + \mathbf{q}_3| = \sqrt{E_1^2 + E_3^2 + 2E_1 E_3 \cos\theta}. \quad (26)$$

We may then write $d^3\mathbf{q}_1 = 2\pi E_1^2 d|\mathbf{q}_1| d\cos\theta$, and we have

$$d\Gamma = 2\pi K \frac{E_1 E_3 (m_Z - 2E_3)^2}{|\mathbf{q}_1 + \mathbf{q}_3|} d^3\mathbf{q}_3 dE_1 d\cos\theta \delta[g(\cos\theta)], \quad (27)$$

where $g(\cos\theta) = m_Z - E_1 - E_2(\cos\theta) - E_3$.

Now, the delta function cannot be directly integrated, so we need to change variables. This redefinition leads to

$$\delta[g(\cos\theta)] = \frac{E_2(\cos\theta)}{E_1 E_3} \delta(\cos\theta - \cos\theta_0), \quad (28)$$

where $\cos\theta_0$ is such that $g(\cos\theta_0) = 0$. The delta function now implies that both the maximum energy of any individual photon and the minimum energy of any pair of photons are $m_Z/2$. Consequently, we have E_1 and E_3 limited to the ranges $(\frac{m_Z}{2} - E_3, \frac{m_Z}{2})$ and $(0, \frac{m_Z}{2})$, respectively. Performing the remaining integrations and dividing by the Z -boson width, we find that the branching ratio is given by

$$\begin{aligned} \text{BR}(Z \rightarrow 3\gamma)_Y &= \frac{s_\theta^2 c_\theta^6}{184320\pi^3 \Gamma_{\text{exp}}^Z} \frac{m_Z^9}{\beta^4} \\ &= 6.7 \times 10^{-7} \left(\frac{m_Z}{\sqrt{\beta}} \right)^8. \end{aligned} \quad (29)$$

We are finally able to place an experimental bound on β . The branching ratio predicted by the SM is extremely small ($\sim 10^{-10}$), way below current experimental sensitivities. If the expression above fully saturates the experimental upper limit, i.e., $\text{BR}(Z \rightarrow 3\gamma)_Y \simeq \text{BR}(Z \rightarrow 3\gamma)_{\text{exp}}$; cf. Eq. (14), we find that

$$\sqrt{\beta} \gtrsim 80 \text{ GeV}, \quad (30)$$

which is slightly lower than the bound reported in Ref. [28]. In Ref. [41], the authors adopt the result of Eq. (30) above on the BI parameter to make estimates on the redshift and to discuss birefringence and dichroism in connection with a class of p-extended BI-type actions in the presence of an external uniform magnetic field.

Here, we must add an important remark. The energy scale of a decay process is set by the mass of the decaying particle, here given by $m_Z = 91.2 \text{ GeV}$. Therefore, the bound obtained above must be taken with a grain of salt since it represents a mass scale lower than the energy of the process, challenging the basic assumption behind our effective-theory approach. Nonetheless, it is worth noticing that this restriction is a matter of experimental limitation: the best bound on the Z -decay into three photons is still orders of magnitude away from the SM prediction, so we may confidently expect that future experiments will yield much more stringent bounds on it, therefore significantly improving on the result above.

The lower bound in Eq. (30) is clearly limited by the experimental sensitivity. If the current experimental upper bound on the branching ratio [cf. Eq. (14)] would be improved by a factor of ~ 3 —a smaller improvement than the one from ATLAS [36] relative to LEP [37]—we would be able to exclude the region $\sqrt{\beta} \lesssim m_Z$. Future lepton colliders, e.g., ILC [42–45] and FCC-ee [46,47], whose main goal is precision Higgs physics, could operate at the Z -pole and produce a vast sample of Z -bosons; the ILC and the FCC-ee could produce, respectively, 10^2 and 10^5 times more Z -bosons than LEP. It is therefore possible, with much better statistics and improved detector capabilities, to improve the upper limit on $\text{BR}(Z \rightarrow 3\gamma)$ enough to constrain $\sqrt{\beta}$ at or above m_Z .

In Fig. 2, we plot the lower bound on $\sqrt{\beta}$ as a function of the future improvement of the experimental sensitivity, $\text{BR}(Z \rightarrow 3\gamma)_{\text{exp}}$, relative to the currently best one [36]. The situation discussed in the paragraph above is illustrated by the area shaded in red; an improvement of at least ~ 3 would lead to viable bounds. The unfortunately weak dependence of the expansion parameter on the experimental sensitivity is made explicit by the slope of the curve, meaning that

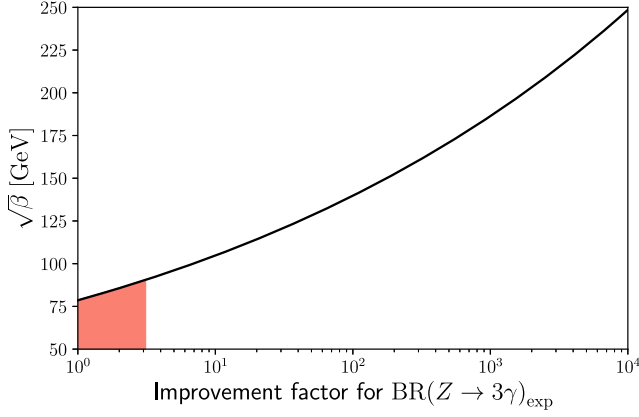


FIG. 2. Projection for the lower bound on $\sqrt{\beta}$ as a function of the improvement factor of the experimental sensitivity relative to the currently best one; cf. Eq. (14) [36]. Incidentally, Eq. (29) reaches the order of magnitude of the SM prediction with $\sqrt{\beta} \sim 220$ GeV. The region shaded in red is such that $\sqrt{\beta} < m_Z$, where our predictions are not accurate.

only large improvements in sensitivity would lead to noticeable improvements in the lower bound on our nonlinear extension.

As a final remark, we note that the discussion above relies on the fact that, so far (and in the foreseeable future), only upper limits on the process $Z \rightarrow 3\gamma$ could be placed. The SM prediction is 4 orders of magnitude below the currently best upper bound, so we may also speculate about possible limits on the expansion parameter in case the SM expectation is eventually confirmed. In this scenario, there is no tension between the SM and experiment, so we may assume that the nonstandard result is responsible for a small correction of the SM prediction, being hidden under the (relative) experimental uncertainty, i.e., $\text{BR}_Y(\beta)/\text{BR}_{\text{SM}} \lesssim \delta_{\text{exp}}$. Conservatively assuming $\delta_{\text{exp}} \sim 10\%$ would allow us to improve the lower bound to $\sqrt{\beta} \gtrsim 295$ GeV. For even better precisions of 1% and 0.1%, we find $\sqrt{\beta} \gtrsim 395$ GeV and $\sqrt{\beta} \gtrsim 530$ GeV, respectively.

B. $e^-e^+ \rightarrow 3\gamma$

Hadron colliders have played a central role in the establishment of the SM as our best theory of elementary particles and their interactions; great examples are the discoveries of the W- and Z-bosons, as well as of the Higgs scalar. However, lepton colliders, such as LEP, were crucial in subsequent precision measurements, helping to probe not only tree-level predictions but also radiative corrections [48]. The next development is to achieve even higher precision in measurements of electroweak parameters, in particular those related to the Higgs and gauge bosons [49].

Lepton colliders represent optimal tools to this end, and next-generation machines have been proposed, such as ILC [42–45], FCC-ee [46,47], CEPC [50], and CLIC [51].

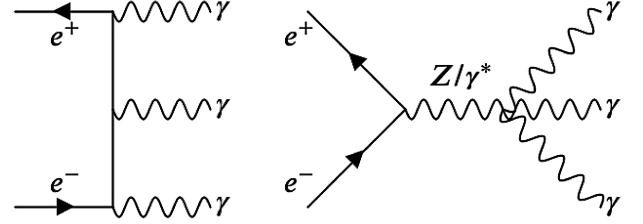


FIG. 3. The lowest-order Feynman diagrams contributing to the scattering $e^-(p_1)e^+(p_2) \rightarrow \gamma(q_1)\gamma(q_2)\gamma(q_3)$.

These are designed to study the SM in great detail, but searching for deviations from the SM that could hint at new physics is an equally important goal. In this context, the process $e^-e^+ \rightarrow 3\gamma$ offers an interesting option to test modifications of the gauge couplings, in particular those involving photons and Z-bosons. From Eq. (13), we see that our nonlinear extension induces precisely such anomalous couplings that could give rise to new contributions for processes with three photons in the final state. We note that the SM contribution is very well described by QED with negligible electroweak corrections.

The Feynman diagrams contributing to $e^-e^+ \rightarrow 3\gamma$ at tree level are shown in Fig. 3. The QED contribution is given by

$$-i\mathcal{M}_{\text{QED}} = ie^3 \bar{v}(p_2) \left[\gamma^\rho \frac{\not{p}_1 - \not{q}_1 - \not{q}_2}{(p_1 - q_1 - q_2)^2} \gamma^\nu \times \frac{\not{p}_1 - \not{q}_1}{(p_1 - q_1)^2} \gamma^\mu \right] u(p_1) \epsilon_\mu^*(q_1) \epsilon_\nu^*(q_2) \epsilon_\rho^*(q_3), \quad (31)$$

which must be added to the other five amplitudes obtained from this one by permutation of the external photons. We are considering high-energy scatterings, so the electron mass may be safely neglected. The nonlinearly induced photon- and Z-mediated amplitudes are given by

$$-i\mathcal{M}_\gamma = \frac{-e}{(p_1 + p_2)^2} \bar{v}(p_2) \gamma_\mu u(p_1) \times V_{4\gamma}^{\mu\nu\beta\rho}(\beta) \epsilon_\nu^*(q_1) \epsilon_\beta^*(q_2) \epsilon_\rho^*(q_3), \quad (32)$$

$$-i\mathcal{M}_Z = \frac{g_Z}{(p_1 + p_2)^2 - m_Z^2 + im_Z \Gamma_Z} \times \bar{v}(p_2) \gamma_\mu (c_v - c_a \gamma^5) u(p_1) \times V_{Z3\gamma}^{\mu\nu\beta\rho}(\beta) \epsilon_\nu^*(q_1) \epsilon_\beta^*(q_2) \epsilon_\rho^*(q_3), \quad (33)$$

where $g_Z = e/4s_\theta c_\theta$, $c_v = -1 + 4s_\theta^2$ and $c_a = -1$. The Z-width is $\Gamma_Z = 2.49$ GeV. The $Z\gamma\gamma\gamma$ vertex was defined in Eq. (16), and the four-photon vertex is analogous:

$$V_{4\gamma}^{\alpha\beta\gamma\delta}(\beta) = i \frac{c_\theta^4}{\beta^2} f^{\alpha\beta\gamma\delta}. \quad (34)$$

The function $f^{\alpha\beta\gamma\delta}$ is given by Eq. (17) with the appropriate relabeling of the 4-momenta.

The total tree-level amplitude for the process, \mathcal{M} , is $\mathcal{M} = \mathcal{M}_{\text{QED}} + \mathcal{M}_\gamma + \mathcal{M}_Z$, and the total unpolarized cross section is given by

$$d\sigma = \frac{1}{3!} \frac{1}{2E_{\text{cm}}^2} \langle |\mathcal{M}|^2 \rangle d\Pi_3, \quad (35)$$

where $1/3!$ is the symmetry factor due to the identical photons in the final state and the phase-space factor is the same as in Eq. (23). The squared amplitude is essentially the sum of three contributions: a pure QED part, an interference term between QED and the nonlinear amplitudes, and a purely nonlinear term. The contribution from pure QED is discussed in the Appendix A.

Let us first discuss the interference term, $\langle |\mathcal{M}|_{\text{QED-Y}}^2 \rangle$. The unpolarized squared amplitude is quoted in detail in Appendix B. To simplify matters, we may express all energies and 3-momenta in units of the c.m. energy, E_{cm} , so that we can write it as

$$\langle |\mathcal{M}|_{\text{QED-Y}}^2 \rangle = \mathcal{X}_{\text{QED-Y}} e^4 c_\theta^2 \frac{E_{\text{cm}}^2}{\beta^2} \mathcal{A}(p_i, q_j), \quad (36)$$

with $\mathcal{A}(p_i, q_j)$ representing a function of the now dimensionless energies and 3-momenta that the reader may obtain from Eq. (B1). The prefactor $\mathcal{X}_{\text{QED-Y}}$ is given by ($x = m_Z^2/E_{\text{cm}}^2$ and $y = \Gamma_Z^2/m_Z^2$)

$$\mathcal{X}_{\text{QED-Y}} = \frac{3 - (3 + 4c_\theta^2)x + 4c_\theta^2 x^2(1 + y)}{(1 - x)^2 + yx^2}. \quad (37)$$

From the phase-space volume, we get another factor of E_{cm}^2 that cancels the one present in the denominator of Eq. (35), so that, putting all the numerical factors together, we finally obtain

$$\sigma(e^-e^+ \rightarrow 3\gamma)_{\text{QED-Y}} = \mathcal{X}_{\text{QED-Y}} \frac{\alpha^2 c_\theta^2 s}{384\pi^3 \beta^2} \mathcal{I}_{\text{QED-Y}} \quad (38)$$

with $s = E_{\text{cm}}^2$, $e^2 = 4\pi\alpha$ and

$$\mathcal{I}_{\text{QED-Y}} = \int \mathcal{A}(p_i, q_j) \frac{d^3\mathbf{q}_1}{E_1} \frac{d^3\mathbf{q}_2}{E_2} \frac{d^3\mathbf{q}_3}{E_3} \delta^4(\Sigma p_i - \Sigma q_j). \quad (39)$$

Note that the quantities in Eq. (39) are all expressed in units of $\sqrt{s} = E_{\text{cm}}$, being therefore dimensionless.

Equation (39) cannot be easily evaluated analytically due to the complexity of the integrand, so we solve it numerically via standard Monte Carlo methods. The Dirac delta enforcing 4-momentum conservation severely constrains the phase-space volume available to the outgoing photons. In fact, their individual energies are bound to be at most 0.5, and the sum of any pair of energies must be larger than this value, allowing us to limit the range of the sampled 3-momentum components to the interval $[-0.5, 0.5]$. In what follows, we use data from e^-e^+ collisions at LEP resulting in two or three

TABLE I. Values of the numerical integrals appearing in Eqs. (38), (43), and (A7). The first two energy values are relevant in the context of existing LEP data [52,53], whereas the last two are important for future e^-e^+ colliders, such as the ILC [42–45,54]. The following cuts were applied: $E_\gamma > 5$ GeV and $|\cos\theta_\gamma| < 0.96$ [52,53].

\sqrt{s} (GeV)	91.2	207	250	350
\mathcal{I}_{QED}	27006	37976	41796	45854
$\mathcal{I}_{\text{QED-Y}}$	19.45	20.02	20.13	20.24
\mathcal{I}_Y	0.138	0.139	0.139	0.139

photons, and the cross sections quoted were obtained under the experimental conditions of the detector. That means that we have to impose similar cuts to our theoretical cross sections if we want to compare them to LEP data.

Particularly important are the angular and energy cuts imposed [52,53]. Since the forward-backward direction along the beam is inaccessible, the range in polar angles is limited to $16^\circ \leq \theta_\gamma \leq 164^\circ$, i.e., the detectable photons must satisfy $|\cos\theta_\gamma| \leq 0.96$ to be contained in the electromagnetic calorimeter. Furthermore, the individual photons must have an energy $E_\gamma > 5$ GeV. Even though Eq. (39) is written in terms of dimensionless quantities, the aforementioned lower threshold on the detectable energy of the single photons introduces an energy dependence, as the cut is expressed as $E_\gamma > 5/\sqrt{s}$. The values of the integral evaluated at selected energy values are quoted in Table I. For the sake of concreteness, the interference cross section at $\sqrt{s} = 207$ GeV is

$$\sigma_{\text{QED-Y}}(\sqrt{s} = 207 \text{ GeV}) \simeq 0.88 \left(\frac{250 \text{ GeV}}{\sqrt{\beta}} \right)^4 \text{ fb}. \quad (40)$$

We now move on to the purely nonlinear contribution, $\langle |\mathcal{M}|_Y^2 \rangle$, which is expected to be subdominant relative to the interference term discussed above. The unpolarized squared amplitude is stated in Eq. (B5), and after expressing the 4-momenta in units of E_{cm} , we have

$$\langle |\mathcal{M}|_Y^2 \rangle = \mathcal{X}_Y e^2 c_\theta^4 \frac{E_{\text{cm}}^6}{\beta^4} \mathcal{B}(p_i, q_j), \quad (41)$$

with $\mathcal{B}(p_i, q_j)$ representing a dimensionless function in analogy with $\mathcal{A}(p_i, q_j)$. The prefactor is

$$\mathcal{X}_Y = \frac{5 - 12c_\theta^2 x + 8c_\theta^4 x^2(1 + y)}{(1 - x)^2 + yx^2}. \quad (42)$$

Equation (41) may be integrated analytically,¹ but here we adopted the same Monte Carlo setup employed in the calculation of the interference term. The cross section is then given by

¹The result without detector cuts is $\sigma_Y = \mathcal{X}_Y \frac{\alpha c_\theta^4 s^3}{368640\pi^2 \beta^3}$.

$$\sigma(e^-e^+ \rightarrow 3\gamma)_Y = \mathcal{X}_Y \frac{\alpha c_\theta^4}{6144\pi^4} \frac{s^3}{\beta^4} \mathcal{I}_Y, \quad (43)$$

where \mathcal{I}_Y is defined analogously to $\mathcal{I}_{\text{QED-Y}}$; cf. Eq. (39). Specializing to $\sqrt{s} = 207$ GeV and using the numerical value of the integral including detector cuts from Table I, we have

$$\sigma_Y(\sqrt{s} = 207 \text{ GeV}) \simeq 0.01 \left(\frac{250 \text{ GeV}}{\sqrt{\beta}} \right)^8 \text{ fb}. \quad (44)$$

In the discussion above, we have obtained the total cross sections involving the novel neutral vertices originating in Eq. (13). The fact that only quartic vertices are produced implies that $e^-e^+ \rightarrow 2\gamma$ does not receive corrections, at least at tree level, but $e^-e^+ \rightarrow 3\gamma$ does. From dimensional analysis alone, we expect the number of events with two photons to be roughly 2 orders of magnitude times larger than with three photons, thus making dedicated searches for three-photon events harder. Therefore, more commonly, experiments look for multiphoton processes, and the best available data to our knowledge were collected at LEP where the c.m. energy of the e^-e^+ pair was scanned passing by the Z-pole and reaching more than 200 GeV.

The L3 Collaboration analyzed LEP data of events resulting in multiphoton final states [52,53]. Since electroweak corrections are heavily suppressed, these measurements provide a clean test of QED, whose predictions were successfully confirmed. The calculations of the QED expectation were performed following Ref. [55], where contributions up to $\mathcal{O}(\alpha^3)$ are considered, i.e., the tree-level cross sections for two and three final photons plus radiative corrections. Here, however, we are working with an effective theory, and we limit our analysis to tree level and refrain from employing their results.

The tree-level cross section for $e^-e^+ \rightarrow 2\gamma$ is well known; cf. Eq. (A2). No closed form for the tree-level cross section for $e^-e^+ \rightarrow 3\gamma$ in the CM could be found, so we calculated the squared amplitude analytically and performed the phase-space integration numerically including the appropriate detector cuts; cf. Eq. (A8). Let us consider concrete data to try to constrain $\sqrt{\beta}$. Since we are dealing with an effective theory whose effects grow with energy, we will ignore data at the Z-pole [52] and focus on the more promising high-energy results [53].

The L3 Collaboration analyzed $e^-e^+ \rightarrow \gamma\gamma(\gamma)$ data in detail and indicates cross-section measurements for final states with two and three photons. The highest energy bin is 207 GeV (cf. Table 3 of Ref. [53]), and it quotes the expected $\mathcal{O}(\alpha^3)$ cross section as 9.9 pb, whereas our tree-level result is 9.2 pb. Given that the difference includes radiative contributions deliberately unaccounted for here and possible effects from further selection criteria, we are confident that our calculation delivers a meaningful result for the QED prediction at tree level.

Now, given that QED accurately describes the experimental data, we are only able to find lower bounds on $\sqrt{\beta}$. In fact, we may constrain it by demanding that the effects of the nonlinear extension hide under the relative experimental uncertainty

$$\frac{\sigma_{\text{QED-Y}} + \sigma_Y}{\sigma_{\text{QED}}} \lesssim \delta_{\text{exp}}, \quad (45)$$

with σ_{QED} being the tree-level expectation from QED. The cross sections for final states with two and three photons are, respectively, $\sigma_{\text{QED}}^{2\gamma}$, Eq. (A2), and $\sigma_{\text{QED}}^{3\gamma}$, Eq. (A8). For the sake of concreteness, we focus on the highest energy bin quoted in Table 3 from Ref. [53], $\sqrt{s} = 207$ GeV, for which the relative uncertainty of the measured cross section is $\delta_{\text{exp}} = 0.34/10.16 \simeq 0.034$. Plugging this and $\sigma_{\text{QED}}^{2\gamma} + \sigma_{\text{QED}}^{3\gamma} = 9.2$ pb into Eq. (45), we obtain $\sqrt{\beta} \gtrsim 73$ GeV.

The absolute number of $e^-e^+ \rightarrow 3\gamma$ events is also reported in Ref. [53] for different energies, albeit without the respective experimental uncertainties. Focusing again on $\sqrt{s} = 207$ GeV, the expected tree-level cross section for pure QED is 0.29 pb. At this energy, 29 three-photon events were observed, so we may conservatively assume that the uncertainty is $\sim\sqrt{29} \simeq 5.4$ events. Taking into account the effective integrated luminosity, 87.8 pb⁻¹, this is equivalent to 0.06 pb, so that the relative uncertainty is $\delta_{\text{exp}} = 0.06/0.29 \simeq 0.21$. With $\sigma_{\text{QED}} = \sigma_{\text{QED}}^{3\gamma} = 0.29$ pb, Eq. (45) gives $\sqrt{\beta} \gtrsim 97$ GeV.

The bounds found above suffer from the same limitation as the one from the analysis of Z-decay: $\sqrt{\beta} < \sqrt{s}$. This is, however, not surprising, since the experimental uncertainties are orders of magnitude larger than the typical values expected from Eqs. (40) and (44). We are thus confronted with the fact that the currently available data on $e^-e^+ \rightarrow \gamma\gamma(\gamma)$ do not yield viable bounds on $\sqrt{\beta}$.

Despite being experimentally more challenging, measuring $e^-e^+ \rightarrow 3\gamma$ has the largest potential, as only the process directly affected by the nonlinear effects is examined. We conclude, therefore, that a sensible lower limit on $\sqrt{\beta}$ could be placed if future e^-e^+ colliders would include measuring this process in their research programs. Let us take the ILC as an example, which targets a total integrated luminosity of 14 ab⁻¹ over its full operation time [54]. For the sake of clarity, let us focus on the initial stage with $\sqrt{s} = 250$ GeV, where an integrated luminosity of ~ 500 fb⁻¹ is planned to be attained in the first five years. Assuming similar detector cuts as at LEP and a (pessimistic) 1% effective luminosity,² ~ 5 fb⁻¹, pure QED predicts 1073 three-photon events, whereas the nonlinear terms would contribute with three extra events for $\sqrt{\beta} = 300$ GeV; i.e., the level of precision required would

²For comparison, the analysis of $e^-e^+ \rightarrow \gamma\gamma(\gamma)$ at LEP in the energy range 192–209 GeV contained 0.43 fb⁻¹ of data, roughly ten times less.

be $3/1073 \sim 0.3\%$. A similar precision would be required at $\sqrt{s} = 350$ GeV with $\sqrt{\beta} = 400$ GeV.

C. Pure gauge-boson scatterings

The electroweak sector of the SM is based on the non-Abelian gauge group $SU(2)_L \times U(1)_Y$. This is manifest in the form of the covariant derivative; cf. Eq. (4) and the nonlinear transformation properties of the gauge bosons. Particularly relevant is the presence of triple and quartic self-interaction couplings in the gauge sector. As a matter of fact, in a pure Yang-Mills theory, the quartic coupling is related to the triple one, even at the quantum level, as a consequence of gauge symmetry—this is a trademark feature of a non-Abelian gauge theory. Given that the structure of the gauge self-couplings in the electroweak sector is completely specified by construction, any deviations from this would suggest the presence of new physics.

Measurements of the gauge self-couplings are therefore especially interesting from both theoretical and experimental points of view. Particularly important are high-energy scattering processes involving the Z-boson and the photon, which could give a clear signal indicating SM extensions modifying the hypercharge sector like the one proposed here. With this in mind, we consider some of the possible scattering processes proceeding via the quartic couplings from Eq. (13) already at tree level, instead of loop level as predicted by the SM.

As mentioned in Sec. III B, e^-e^+ colliders offer clean conditions for precision tests of the SM. More interestingly, there are currently proposals of machines that can be adapted to work as linear photon colliders. Important sources of photons at a linear lepton collider include bremsstrahlung [56] and Compton laser backscattering [57] (there is also beamstrahlung [58]). At LEP or LHC bremsstrahlung is the dominating form of radiation production, whereas at TESLA [59], ILC [42,60], or CLIC [51,61,62], Compton backscattering of electrons in intense lasers would be used to produce $\gamma\gamma$ or $e\gamma$ collisions. In this scenario, the photons created may carry a substantial amount of the electron energy [63].

Given that future linear e^-e^+ machines envision in their prospects the possibility of an extension to include photon colliders at relatively low cost, let us focus on $\gamma\gamma$ collisions producing exclusively vector bosons $V_i = \gamma, Z, W^\pm$. In this context, measuring, e.g., the process $\gamma\gamma \rightarrow W^+W^-$ in a photon collider is an attractive option due to its large (~ 80 pb) cross section [64,65]. The nonlinear realization of the hypercharge sector proposed in this work, however, does not affect charged gauge bosons, so we shall focus on $\gamma\gamma$ fusion leading to neutral gauge bosons as final products: $\gamma\gamma \rightarrow \gamma Z$, $\gamma\gamma \rightarrow ZZ$, and $\gamma\gamma \rightarrow \gamma\gamma$. It is noteworthy that, within the SM framework, these processes receive only loop-level contributions, but here they will be induced at tree level by the effective operators present in Eq. (13).

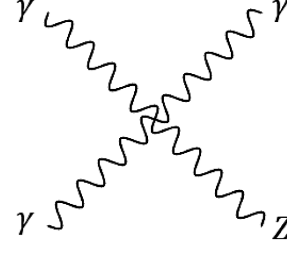


FIG. 4. The lowest-order Feynman diagram contributing to the scattering $\gamma(p_1)\gamma(p_2) \rightarrow \gamma(q_1)Z(q_2)$.

For the sake of concreteness, in the following, we compute the nonlinear contribution to the unpolarized cross section of the process $\gamma\gamma \rightarrow \gamma Z$ at tree level. Though we consider this particular process in more detail, all others may be analyzed by similar means. From Eq. (13), we see that the relevant vertex factor is $V_{Z3\gamma}^{\alpha\beta\gamma\delta}$, cf. Eqs. (16) and (17), but with the substitutions: $p \rightarrow p_1$, $q_1 \rightarrow -p_2$, $q_2 \rightarrow q_1$, and $q_3 \rightarrow q_2$ appropriate for a 2-to-2 scattering.

The tree-level amplitude for this process is then

$$-i\mathcal{M} = \epsilon_\alpha(p_1)\epsilon_\beta(p_2)V_{Z3\gamma}^{\alpha\beta\gamma\delta}(\beta)\epsilon_\gamma^*(q_1)\epsilon_\delta^*(q_2) \quad (46)$$

with the momenta attributions given in Fig. 4. Here, we are assuming that the unpolarized photons are on shell and monochromatic.³ After summing and averaging over polarizations, the unpolarized squared amplitude becomes

$$\langle |\mathcal{M}|^2 \rangle = \frac{c_\theta^6 s_\theta^2}{8\beta^4} [m_Z^4(s^2 + t^2 + u^2) - 2m_Z^2(s^3 + t^3 + u^3) + s^4 + t^4 + u^4], \quad (47)$$

where the Mandelstam variables, expressed in terms of the c.m. energy E_{cm} of the incoming photons and the scattering angle θ , are

$$s = E_{\text{cm}}^2, \quad (48a)$$

$$t = -\frac{1}{2}(E_{\text{cm}}^2 - m_Z^2)(1 - \cos\theta), \quad (48b)$$

$$u = -\frac{1}{2}(E_{\text{cm}}^2 - m_Z^2)(1 + \cos\theta). \quad (48c)$$

Setting $x = m_Z^2/s$, the unpolarized differential cross section for the scattering $\gamma\gamma \rightarrow \gamma Z$ reads

$$\frac{d\sigma}{d\Omega} = \frac{c_\theta^6 s_\theta^2}{4096\pi^2 \beta^4} s^3 (1-x)^3 [(6-2x^2)\cos^2\theta + (1-x)^2\cos^4\theta + 9 + 2x + x^2], \quad (49)$$

³This is a simplified scenario, and a more detailed analysis would follow the strategy from Ref. [28], for example.

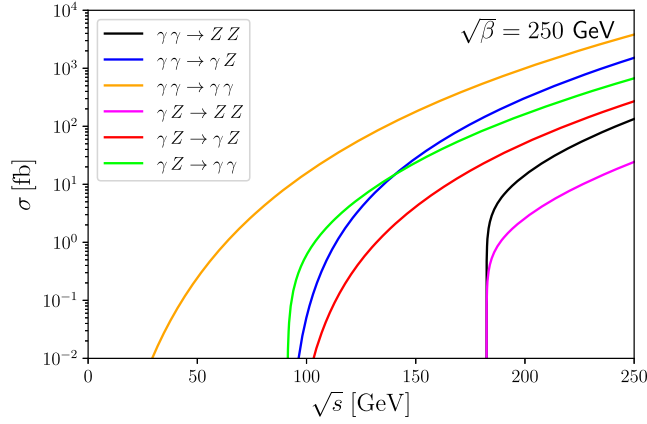


FIG. 5. Unpolarized total cross sections for selected processes (no angular cuts applied; evaluated in the c.m.); cf. Table II. Here, we set $\sqrt{\beta} = 250$ GeV for definiteness, but the scaling for other values can be easily performed via Eq. (51).

which can be integrated to yield

$$\sigma(\gamma\gamma \rightarrow \gamma Z)_\gamma = \frac{s_\theta^2 c_\theta^6}{1920\pi} \left(\frac{s^3}{\beta^4}\right) (1-x)^3 (21 + 3x + x^2). \quad (50)$$

This result is shown in blue in Fig. 5 for $\sqrt{\beta} = 250$ GeV. If the nonlinear hypercharge sector is indeed realized in nature, the expression above would provide the only tree-level contribution to the cross section, since this process cannot take place in the SM at this order. In fact, the first SM contribution is generated via fermion and W-boson loops with a cross section of $\sim 3 \times 10^{-4}$ fb shortly above threshold and peaking at ~ 110 fb at ~ 750 GeV [66].

Another process of interest in a photon collider is $\gamma\gamma \rightarrow ZZ$, which, similar to $\gamma\gamma \rightarrow W^+W^-$, may be used to study the gauge structure of the SM as well as Higgs physics. As already mentioned, this process has no tree-level contribution in the SM—the first nontrivial amplitude arises through fermion and W-boson loops with a cross section of ~ 20 fb immediately after threshold and roughly saturating at ~ 300 fb for c.m. energies $\gtrsim 800$ GeV [59,67,68]. In our nonlinear extension, the first nonzero contribution is at tree level, and the calculation of the (differential) cross section follows a rationale similar to the one leading to Eq. (50). The result is listed in Table II and shown in black in Fig. 5.

Finally, let us briefly comment on $\gamma\gamma \rightarrow \gamma\gamma$, light-by-light (LbL) scattering. In Maxwell’s linear electromagnetism, this process is forbidden, but in the 1930s, Heisenberg and Halpern [1,2] realized that quantum effects could induce it. In the 1950s, a full calculation was presented [69], and the cross section was found to be $\sim 10^{-34}$ pb for visible light [70,71]. Only recently, it was proposed that this elusive process could be observed at the LHC in Pb-Pb collisions [72]—in fact, strong evidence for it has been reported by the ATLAS [15] and CMS collaborations [16], being

TABLE II. Total cross sections for processes involving only quartic couplings of neutral gauge bosons; cf. Eq. (51) with $x = m_Z^2/s$. These results are shown in Fig. 5 for $\sqrt{\beta} = 250$ GeV.

Process	N	$\kappa(x)$	$F(x)$
$\gamma\gamma \rightarrow \gamma\gamma$	$\frac{7c_\theta^8}{1280\pi}$	1	1
$\gamma\gamma \rightarrow \gamma Z$	$\frac{s_\theta^2 c_\theta^6}{1920\pi}$	$(1-x)^3$	$21 + 3x + x^2$
$\gamma\gamma \rightarrow ZZ$	$\frac{s_\theta^4 c_\theta^4}{1280\pi}$	$\sqrt{1-4x}$	$7 - 26x + 27x^2$
$\gamma Z \rightarrow \gamma\gamma$	$\frac{s_\theta^2 c_\theta^6}{5760\pi}$	$(1-x)$	$21 + 3x + x^2$
$\gamma Z \rightarrow \gamma Z$	$\frac{s_\theta^4 c_\theta^4}{2880\pi}$	$(1-x)^4$	$21 + 6x + 16x^2 + 6x^3 + 6x^4$
$\gamma Z \rightarrow ZZ$	$\frac{s_\theta^6 c_\theta^2}{5760\pi}$	$(1-x)\sqrt{1-4x}$	$21 - 75x + 98x^2 - 20x^3 + 6x^4$

further confirmed by ATLAS [17]. The results are compatible with the SM prediction. As with the other photon-fusion processes previously discussed, LbL scattering takes place only at loop level in the SM. Our nonlinear extension, on the other hand, allows for it to proceed already at tree level and with a potentially large cross section; cf. Fig. 5.

The quartic vertices in Eq. (13) allow for a few more tree-level scattering processes involving exclusively neutral gauge bosons than we have explicitly mentioned above. For the sake of completeness, the differential cross sections for these processes are given in Appendix C, and the respective total cross sections, without any angular cuts, can be written in a systematic way as

$$\sigma = N \left(\frac{s^3}{\beta^4}\right) \kappa(x) F(x) \quad (51)$$

with $x = m_Z^2/s$. Here, N is a numerical factor, $\kappa(x)$ is a kinematic and phase-space factor, and further energy-dependent contributions are contained in $F(x)$. These results are summarized in Table II and shown in Fig. 5 for a reference value of $\sqrt{\beta} = 250$ GeV. The basic features are immediately salient: besides LbL scattering, all cross sections sharply rise after the respective thresholds and grow with increasing c.m. energy, as expected from the effective character of our hypercharge extension.

It is important at this point to contextualize our findings with recent results on anomalous quartic gauge couplings (aQGC). In fact, it is interesting to discuss experimental bounds and projected sensitivities on aQGC, as these may be translated into constraints on the parameter β from different, but complementary, perspectives, ranging from past LHC runs to future lepton colliders. Particularly relevant is the discussion of recent results related to the anomalous vertices $\gamma\gamma Z$ and $\gamma\gamma\gamma\gamma$.

Anomalous quartic gauge couplings can be investigated with high precision at the LHC through $pp \rightarrow pXp$ processes, where X can be, for instance, $\gamma\gamma$ or γZ . In particular, it is interesting to focus on photon-induced processes in pp collisions since these processes are very

sensitive to aQGC and therefore new physics beyond the SM (e.g., extended Higgs sectors or extra dimensions).

For instance, the $\gamma\gamma Z$ interaction appears in the SM through fermion and W -boson loops. This anomalous vertex induces the rare decay $Z \rightarrow \gamma\gamma\gamma$, contributes to $e^+e^- \rightarrow \gamma\gamma\gamma$ and allows also for the $\gamma\gamma \rightarrow \gamma Z$ scattering. New physics appearing at a mass scale Λ , much heavier than the experimentally accessible energies E , can have its effects described via a low-energy effective field theory. The anomalous $\gamma\gamma\gamma Z$ interaction could then be parametrized by dimension-8 operators such as

$$\mathcal{L}_{Z3\gamma}^{(1)} = \zeta F^{\mu\nu} F_{\mu\nu} F^{\rho\sigma} Z_{\rho\sigma} + \tilde{\zeta} F^{\mu\nu} \tilde{F}_{\mu\nu} F^{\rho\sigma} \tilde{Z}_{\rho\sigma}. \quad (52)$$

This is an effective description, and we recover our model by making $\zeta = \tilde{\zeta} = -\frac{1}{8\beta^2} s_\theta c_\theta^3$.

Baldenegro *et al.* studied in great detail the γZ production with intact protons in the forward region at the LHC using proton tagging [73]. In this way, a sensitivity of $\zeta < 2 \times 10^{-13} \text{ GeV}^{-4}$ could be established for the anomalous quartic gauge coupling $\gamma\gamma\gamma Z$ at an integrated luminosity of 300 fb^{-1} . This improves the result obtained through the $Z \rightarrow \gamma\gamma\gamma$ measurement by about 3 orders of magnitude. This improvement in the anomalous coupling sensitivity would, in turn, translate into an improvement on the sensitivity of $\sqrt{\beta}$, putting it at the order of a few hundred GeV.

Recently, Inan and Kisselev studied very carefully the $\gamma\gamma \rightarrow \gamma Z$ scattering of photons produced by Compton backscattering at the CLIC and estimated the sensitivity to the anomalous quartic coupling $\gamma\gamma\gamma Z$ [74]. They used the following parametrization:

$$\mathcal{L}_{Z3\gamma}^{(2)} = g_1 F^{\rho\mu} F^{\alpha\nu} \partial_\rho F_{\mu\nu} Z_\alpha + g_2 F^{\rho\mu} F_\mu^\nu \partial_\rho F_{\alpha\nu} Z^\alpha. \quad (53)$$

We can relate these coefficients with the previous ones through $g_1 = 8(\tilde{\zeta} - \zeta)$ and $g_2 = 8\tilde{\zeta}$. The authors considered both polarized and unpolarized e^+e^- collisions at 1.5 and 3 TeV, obtaining exclusion limits on the aQGCs and comparing their results with the previous bounds obtained from γZ production at the LHC. The best bounds found by the authors for the couplings $g_{1,2}$ were approximately $4.4 \times 10^{-14} \text{ GeV}^{-4}$ and $5.1 \times 10^{-15} \text{ GeV}^{-4}$ for the e^+e^- energies 1.5 and 3 TeV, respectively. They conclude that the sensitivities on the anomalous couplings obtained at CLIC are roughly 1 to 2 orders of magnitude stronger than the limits that can be obtained at the LHC. Such an improvement would be enough to put the sensitivity on our nonlinear parameter $\sqrt{\beta}$ at the TeV scale.

Let us now move on to the anomalous coupling $\gamma\gamma\gamma\gamma$. We can describe the nonlinear effects on LbL scattering by means of the following effective Lagrangian:

$$\mathcal{L}_{4\gamma}^{(1)} = \zeta_1 F_{\mu\nu} F^{\mu\nu} F_{\rho\sigma} F^{\rho\sigma} + \zeta_2 F_{\mu\nu} F^{\nu\rho} F_{\rho\sigma} F^{\sigma\mu}. \quad (54)$$

This can be related to our description if we write it in a different, but equivalent, basis given by

$$\mathcal{L}_{4\gamma}^{(2)} = \xi F_{\mu\nu} F^{\mu\nu} F_{\rho\sigma} F^{\rho\sigma} + \tilde{\xi} F_{\mu\nu} \tilde{F}^{\mu\nu} F_{\rho\sigma} \tilde{F}^{\rho\sigma}, \quad (55)$$

where the relation between the above parameters is given by $\xi = \zeta_1 + \frac{1}{2}\zeta_2$ and $\tilde{\xi} = \frac{1}{4}\zeta_2$. We can recover our model if we take the particular combination $\xi = \tilde{\xi} = \frac{c_\theta^3}{32\beta^2}$.

Fichet *et al.* analyzed the sensitivities to the anomalous coupling $\gamma\gamma\gamma\gamma$ at the LHC through diphoton production with intact outgoing protons [75,76]. The reported limits at 14 TeV with an integrated luminosity of $L = 300 \text{ fb}^{-1}$ on $|\zeta_1|$ and $|\zeta_2|$ were $1.5 \times 10^{-14} \text{ GeV}^{-4}$ and $3.0 \times 10^{-14} \text{ GeV}^{-4}$, respectively. For the High-Luminosity LHC (HL-LHC), the sensitivities obtained were a factor of 2 stronger. These results are strong and can put the sensitivity on our $\sqrt{\beta}$ at the TeV scale.

Inan and Kisselev examined the anomalous couplings $\gamma\gamma\gamma\gamma$ in the polarized LbL scattering at CLIC [77]. Their results at 1.5 TeV were comparable with the bound obtained at HL-LHC stated above, but their results for 3 TeV were approximately 1 order of magnitude stronger, improving further the sensitivity on $\sqrt{\beta}$ but still keeping it at the TeV scale. A similar result could be found considering the best sensitivities on the anomalous couplings obtained through $\gamma\gamma \rightarrow ZZ$ in Ref. [78] and also through $Z\gamma\gamma$ production in Ref. [79], both considering e^+e^- collisions at 3 TeV at CLIC.

Finally, let us conclude this section by reporting the latest experimental results on the anomalous couplings of interest here. A more general effective description including the nine independent dimension-8 operators respecting the $SU(2)_L \times U(1)_Y$ gauge symmetry as well as charge conjugation and parity invariance can be found in Ref. [80]. This effective description includes in particular

$$\mathcal{L} \supset F_{T,8} B_{\mu\nu} B^{\mu\nu} B_{\rho\sigma} B^{\rho\sigma} + F_{T,9} B_{\mu\nu} B^{\nu\rho} B_{\rho\sigma} B^{\sigma\mu}. \quad (56)$$

To the best of our knowledge, the strongest experimental bounds on these anomalous couplings are given by the very recent CMS results reported in Refs. [81–84], considering different measurements in proton-proton collisions at $\sqrt{s} = 13 \text{ TeV}$ performed at the LHC. In particular, the strongest bounds on the anomalous couplings $F_{T,8}$ and $F_{T,9}$ are reported in Ref. [84] and give $|F_{T,8}| < 4.7 \times 10^{-13} \text{ GeV}^{-4}$ and $|F_{T,9}| < 9.1 \times 10^{-13} \text{ GeV}^{-4}$. These coefficients are translated into our model by taking $F_{T,8} + F_{T,9}/2 = 1/32\beta^2$ and $F_{T,9}/4 = 1/32\beta^2$. Therefore, these experimental results put the bound on $\sqrt{\beta}$ at the order of a few hundred GeV.

Very recently, a work appeared on the arXiv [85] in which the authors search for exclusive two-photon production via photon exchange in proton-proton collisions, $pp \rightarrow p\gamma\gamma p$, with intact protons using the CMS and TOTEM detectors at a center-of-mass energy of 13 TeV at the LHC. They report the following bounds on the anomalous four-photon coupling parameters: $|\zeta_1| < 2.88 \times 10^{-13} \text{ GeV}^{-4}$ and $|\zeta_2| < 6.02 \times 10^{-13} \text{ GeV}^{-4}$. This would give us a limit on $\sqrt{\beta}$ around the same order of magnitude as the result reported above.

The most recent and strong contribution to the subject was recently given by Ellis *et al.* [86], constraining the nonlinear scale of a BI extension of the SM to be $\gtrsim 5 \text{ TeV}$ considering $gg \rightarrow \gamma\gamma$ at the LHC. The authors estimate the sensitivities at possible future pp colliders with $\sqrt{s} = 100 \text{ TeV}$ to be around $\gtrsim 20 \text{ TeV}$.

Therefore, we conclude that the LHC results can give very strong constraints on aQGC. These can be translated as bounds on $\sqrt{\beta}$ typically at the order of a few hundred GeV up to the TeV scale. Nevertheless, future colliders are expected to be able to supersede these constraints, consequently improving the sensitivity on $\sqrt{\beta}$.

IV. CONCLUSIONS

Motivated by recent results in the physics of electroweak monopoles, we investigated the consequences of a nonlinear extension in the weak hypercharge sector in high-energy processes. The proposed extension is characterized by a parameter $\sqrt{\beta}$ with dimension of mass, which may be used to perform a Taylor expansion in $X = \frac{F}{\beta^2} - \frac{G^2}{2\beta^4}$; cf. Eq. (12). After EW symmetry breaking, we obtain a series of quartic, dimension-8 effective operators involving the photon and Z-boson that are absent from the SM at tree level; cf. Eq. (13).

In this context, we have analyzed a few interesting processes, namely, Z-decay and electron-positron annihilation, both resulting in three photons as final products, and Z-boson production via photon fusion. The first and most promising one, Z-decay, is a rare process occurring only at loop level in the SM, but induced at tree level by nonlinear effects. The expected impact of the nonlinear vertex on the branching ratio is a factor ~ 3 too small; cf. Eq. (29). This is due to the still-loose experimental upper bound on the branching ratio of Z-decay into three photons, which is 4 orders of magnitude larger than the value predicted by the SM.

Future e^-e^+ colliders, such as the ILC or FCC-ee, may operate at the Z-resonance and produce a large amount of Z-bosons—up to a factor 10^5 more than at LEP—thereby dramatically increasing the statistics for measuring the products of Z-decay. We are therefore confident that the experimental upper limit on the branching ratio will be significantly improved in the near future, thus enabling us to set more stringent bounds on $\sqrt{\beta}$, readily excluding the range $\sqrt{\beta} \lesssim m_Z$; cf. Fig. 2. We remark that, in a scenario

where experiment reaches the level of the SM prediction, lower bounds $\sim 300 \text{ GeV}$ could be set.

The second process analyzed was electron-positron annihilation into three photons, also a relatively rare process. It is well described by QED, and the nonlinear extension provides small corrections also at tree level; cf. Fig. 3. We have calculated the unpolarized cross sections of pure QED, pure nonlinear and interference effects at the c.m. Since there is no tension between the predictions from QED and the experimental data, we have used the (relative) experimental uncertainties from LEP data for $e^-e^+ \rightarrow \gamma\gamma(\gamma)$ and $e^-e^+ \rightarrow 3\gamma$ above the Z-pole to derive lower bounds on $\sqrt{\beta}$.

The process with two- and three-photon final states is well measured, but the nonlinear effects, which contribute only to $e^-e^+ \rightarrow 3\gamma$, are shadowed by the much larger QED contribution, $e^-e^+ \rightarrow 2\gamma$. The data on exclusively three-photon final states is not so complete, but a conservative estimate delivers a somewhat better lower bound on $\sqrt{\beta}$. The nonlinear effects are much smaller than the available precision, and it was not possible to obtain viable bounds with the current experimental data, but we project that the necessary improvements may be within the reach of the next-generation lepton colliders.

Finally, we have also analyzed selected scattering processes involving exclusively neutral gauge bosons. The unpolarized tree-level cross sections may reach a few hundred fb at $\sqrt{s} = 200 \text{ GeV}$ for $\sqrt{\beta} = 250 \text{ GeV}$; cf. Fig. 5. These processes are good candidates to detect possible signatures from the nonlinear extension in future experiments, given that they occur only at loop level in the SM, but are induced at tree level via Eq. (13).

In this respect, we also reported recent results giving constraints on anomalous quartic gauge couplings obtained at the LHC considering neutral gauge-boson scatterings. We used them to estimate the corresponding limits on $\sqrt{\beta}$ and found that typically they give us bounds of a few hundred GeV. Furthermore, we analyzed the projections for these anomalous couplings in future lepton colliders and found that they improve the sensitivity on $\sqrt{\beta}$, putting it at the TeV scale.

Quite generally, we expect the nonlinear effects to be heavily suppressed by $\sqrt{\beta}$ —it could reach TeV energies depending on the underlying beyond-the-SM scenario. In this work, we have tried to constrain $\sqrt{\beta}$ with high-energy experiments, and we found that, in order to have any chance to detect such effects, very precise measurements are needed. A good example is the Z-decay in three photons, for which the (minute) SM contribution is generated at loop level, whereas the nonlinear effects contribute already at tree level. This, together with the optimistic prospect of an improved upper limit on the branching ratio, makes this process a very promising way to search for the effects outlined in this work.

This can be contrasted to the situation of electron-positron annihilation: the nonlinear effects are orders of magnitude smaller than the SM results and thus very hard to detect—much like finding a needle in a haystack. We can see this by comparing the magnitudes of the cross sections in Eqs. (40) and (44), ~ 0.9 fb for $\sqrt{\beta} = 250$ GeV, with the size of the experimental uncertainties quoted in Ref. [53], ~ 0.5 pb. Since the nonlinear contributions are much smaller than the uncertainties involved, the only way to make them comparable [*à la* Eq. (45)] is by having $\sqrt{\beta} \lesssim \sqrt{s}$ to effectively enhance the nonlinear effects.

Moreover, we remark that the experimental bounds on anomalous gauge couplings are being updated at a relatively fast pace. Their precise measurement is an extremely important task, since it provides a sensitive probe of new physics. We hope that future colliders will shine a new light on this issue, indicating the path to be followed on high-energy physics.

To conclude our contribution, we remark that a more general implementation of the nonlinear extension of the electroweak sector is possible. Here, we have considered the $U(1)_Y$ sector, but an analogous modification may be performed in the $SU(2)_L$ sector. In this case, the already analyzed neutral sector would receive small modifications, but interesting nonlinear effects would also be induced in the charged sector of the SM. This is the subject of another work to appear soon.

ACKNOWLEDGMENTS

P. D. F. thanks especially G. P. de Brito for interesting discussions and technical support. He is grateful to Natanael C. Costa for discussions about Monte Carlo methods and W. B. de Lima and G. Picanço for helpful discussions. P. C. M. is grateful to S. F. Amato, E. Polycarpo, and D. Kroff for their support. The authors are also grateful to the anonymous referee for his/her helpful suggestions. P. D. F. thanks the Brazilian scientific support agencies, CNPq and FAPERJ, for financial support.

APPENDIX A: TREE-LEVEL QED RESULTS FOR $e^-e^+ \rightarrow \gamma\gamma(\gamma)$

In Sec. III B, we discussed the tree-level effects of the nonlinear extension of the $U(1)_Y$ sector in the process $e^-e^+ \rightarrow \gamma\gamma(\gamma)$. The experimental results from LEP included cross sections with final states of two and three photons subjected to detector cuts in energy and scattering angle, namely, $E_\gamma > 5$ GeV and $|\cos\theta_\gamma| < 0.96$ [52,53], so it is important to understand the tree-level expectation from QED to $e^-e^+ \rightarrow \gamma\gamma$ and $e^-e^+ \rightarrow \gamma\gamma\gamma$ under these conditions.

We start with the simplest case, $e^-e^+ \rightarrow \gamma\gamma$. Since there are two identical particles in the final state and the reaction takes place at the c.m., the two photons carry the same energy as the colliding electron. Assuming monochromatic

beams with energies $\mathcal{O}(100$ GeV), the outgoing photons automatically satisfy the energy cut. The tree-level differential cross section is given by the well-known result

$$\frac{d\sigma_{\text{QED}}^{2\gamma}}{d\cos\theta} = \frac{2\pi\alpha^2}{s} \left(\frac{1 + \cos^2\theta}{1 - \cos^2\theta} \right). \quad (\text{A1})$$

For two identical particles, the polar angle is confined to the range $0 \leq \cos\theta_\gamma \leq 1 - c_{\text{cut}}$, and integrating Eq. (A1) in this range, we find⁴

$$\sigma_{\text{QED}}^{2\gamma} = \frac{2\pi\alpha^2}{s} \left[\log\left(\frac{2 - c_{\text{cut}}}{c_{\text{cut}}}\right) + c_{\text{cut}} - 1 \right]. \quad (\text{A2})$$

For LEP at $\sqrt{s} = 207$ GeV with $c_{\text{cut}} = 0.04$, we get 9.6 pb. It is worth pointing out that the divergence in the forward-backward direction leads to a significant reduction of the total cross section even for small angular cuts.

Let us now move on to the more involved case of $e^-e^+ \rightarrow \gamma\gamma\gamma$. The typical amplitude is given in Eq. (31), which must be added to other five similar contributions with permutations of the photon 4-momenta. If we define $p_{ij} = p_i \cdot q_j$ and $q_{ij} = q_i \cdot q_j$, the squared and spin-averaged amplitude can be written as

$$\langle |\mathcal{M}_{3\gamma}|^2 \rangle = \mathcal{Q} \left[p_{11} \sum_{n=0}^3 (p_1 \cdot p_2)^n \mathcal{Q}_n + \text{perm.} \right] \quad (\text{A3})$$

where “perm.” indicates that we must add the expression with the photon labels reshuffled. The prefactor is

$$\mathcal{Q} = \frac{2e^6}{(p_{11})(p_{12})(p_{13})(p_{21})(p_{22})(p_{23})}, \quad (\text{A4})$$

and the terms in the sum are

$$\mathcal{Q}_0 = p_{12}[p_{13}p_{21}p_{22} + p_{23}(p_{11}p_{22} + p_{23}(p_{22} - q_{12}) + p_{21}(p_{22} + q_{23}))] - p_{11}p_{22}p_{23}q_{23}, \quad (\text{A5a})$$

$$\mathcal{Q}_1 = p_{12}[p_{13}p_{21} - p_{21}(p_{22} - 4p_{23}) + p_{23}(p_{23} - q_{23})] + p_{22}[p_{11}(-p_{22} + p_{23} + q_{23}) - p_{23}q_{12} + p_{22}q_{13} + p_{21}p_{23}], \quad (\text{A5b})$$

$$\mathcal{Q}_2 = -2p_{12}p_{21} - p_{22}(2p_{21} - q_{12} + q_{13} + q_{23}), \quad (\text{A5c})$$

$$\mathcal{Q}_3 = p_{21}. \quad (\text{A5d})$$

The final averaged squared amplitude can be symbolically recast in the form

⁴In order to keep track of the forward-backward enhancement in the ultrarelativistic limit, it is usually imposed that $c_{\text{cut}} = 2m_e^2/s$.

$$\langle |\mathcal{M}_{3\gamma}|^2 \rangle = \frac{e^6}{E_{\text{cm}}^2} \mathcal{C}(p_i, q_j), \quad (\text{A6})$$

where we have expressed all dimensional parameters in terms of the c.m. energy—in this way, $\mathcal{C}(p_i, q_j)$ is effectively dimensionless. Taking into account the phase-space volume, cf. Eq. (23), the integral to be solved is

$$\mathcal{I}_{\text{QED}} = \int \mathcal{C}(p_i, q_j) \frac{d^3 \mathbf{q}_1}{E_1} \frac{d^3 \mathbf{q}_2}{E_2} \frac{d^3 \mathbf{q}_3}{E_3} \delta^4(\Sigma p_i - \Sigma q_j), \quad (\text{A7})$$

but an analytical treatment is cumbersome, so we resort to numerical methods, which also facilitate the application of the detector cuts. The results of the Monte Carlo integral are listed in Table I for a few interesting values of the c.m. energy. The tree-level cross section for $e^-e^+ \rightarrow \gamma\gamma\gamma$ is ($e^2 = 4\pi\alpha$)

$$\sigma_{\text{QED}}^{3\gamma} = \frac{\alpha^3}{48\pi^2 s} \mathcal{I}_{\text{QED}} \simeq 8 \times 10^{-3} \cdot \mathcal{I}_{\text{QED}} \left(\frac{200 \text{ GeV}}{\sqrt{s}} \right)^2 \text{ fb}. \quad (\text{A8})$$

Using $\sqrt{s} = 207 \text{ GeV}$ as an example, we have 0.285 pb.

APPENDIX B: INTERFERENCE AND PURELY NONLINEAR AMPLITUDES FOR $e^-e^+ \rightarrow 3\gamma$

Here, we briefly present the results for the tree-level amplitudes discussed in Sec. III B. The interference amplitude between pure QED and the nonlinear contributions may be written as

$$\langle |\mathcal{M}_{\text{QED-Y}}|^2 \rangle = \mathcal{H} \left[\sum_{n=0}^3 (p_1 \cdot p_2)^n H_n + \text{perm.} \right] \quad (\text{B1})$$

with

$$\mathcal{H} = \frac{c_\theta^2 e^4}{2\beta^2 p_1 \cdot p_2 (p_{11} p_{12} p_{13} p_{21} p_{22} p_{23})} \frac{\mathcal{H}_{\text{num}}}{\mathcal{H}_{\text{den}}} \quad (\text{B2})$$

and

$$\mathcal{H}_{\text{num}} = 2c_\theta^2 m_Z^2 (\Gamma_Z^2 + m_Z^2) - (4c_\theta^2 + 3)m_Z^2 (p_1 \cdot p_2) + 6(p_1 \cdot p_2)^2, \quad (\text{B3a})$$

$$\mathcal{H}_{\text{den}} = m_Z^4 + \Gamma_Z^2 m_Z^2 - 4m_Z^2 (p_1 \cdot p_2) + 4(p_1 \cdot p_2)^2. \quad (\text{B3b})$$

The coefficients in Eq. (B1) are given by

$$H_0 = 2p_{22} [(p_{11})^2 [(p_{13})^3 p_{21} p_{22} + p_{12} (p_{23})^2 (p_{21} q_{23} + p_{22} p_{23}) - p_{12} p_{13} p_{23} (p_{12} p_{21} + p_{21} (q_{23} - 2p_{23}) + p_{22} (p_{23} - q_{13}))] - p_{11} p_{12} p_{13} p_{21} p_{23} (p_{21} q_{23} + p_{22} p_{23}) - (p_{12})^2 (p_{13})^2 (p_{21})^2 p_{23}], \quad (\text{B4a})$$

$$H_1 = -p_{22} \{ 2p_{12} p_{13} (p_{21})^2 p_{22} q_{13} + (p_{11})^2 p_{23} [2(p_{12})^2 (p_{23} + q_{13}) + p_{12} (p_{13} (p_{21} + p_{22}) - 2p_{21} q_{23}) + p_{13} p_{21} p_{22}] + p_{11} p_{21} [2(p_{13})^2 p_{21} p_{22} + p_{12} p_{13} (2(p_{23} q_{12} + q_{13} q_{23}) + p_{21} (p_{23} - 2q_{23})) + 2p_{12} p_{23} q_{13} q_{23}] \}, \quad (\text{B4b})$$

$$H_2 = p_{11} p_{21} [p_{13} p_{22} (2p_{11} q_{23} + p_{23} q_{12}) + p_{12} p_{23} (p_{13} q_{12} + 2p_{21} q_{23})]. \quad (\text{B4c})$$

Finally, the purely nonlinear amplitude is given by

$$\langle |\mathcal{M}_Y|^2 \rangle = \mathcal{J} \left[\sum_{n=0}^3 (p_1 \cdot p_2)^n J_n + \text{perm.} \right], \quad (\text{B5})$$

where

$$\mathcal{J} = \frac{c_\theta^4 e^2}{2\beta^4 (p_1 \cdot p_2)^2} \frac{\mathcal{J}_{\text{num}}}{\mathcal{J}_{\text{den}}}, \quad (\text{B6})$$

with

$$\mathcal{J}_{\text{num}} = 2c_\theta^4 m_Z^2 (\Gamma_Z^2 + m_Z^2) - 6c_\theta^2 m_Z^2 (p_1 \cdot p_2) + 5(p_1 \cdot p_2)^2, \quad (\text{B7a})$$

$$\mathcal{J}_{\text{den}} = m_Z^4 + \Gamma_Z^2 m_Z^2 - 4m_Z^2 (p_1 \cdot p_2) + 4(p_1 \cdot p_2)^2. \quad (\text{B7b})$$

The coefficients in Eq. (B5) are given by

$$J_0 = 3(p_{11})^2 p_{22} p_{23} q_{23} - 6p_{11} p_{12} p_{22} p_{23} q_{13} + 3p_{12} p_{13} (p_{21})^2 q_{23}, \quad (\text{B8a})$$

$$J_1 = 3p_{11} q_{23} (p_{21} q_{23} - 2p_{22} q_{13}) + (p_{11})^2 (q_{23})^2 + (p_{21})^2 (q_{23})^2, \quad (\text{B8b})$$

$$J_2 = q_{12} q_{13} q_{23}. \quad (\text{B8c})$$

APPENDIX C: DIFFERENTIAL CROSS SECTIONS FOR NEUTRAL GAUGE BOSON SCATTERINGS

In this Appendix, we report the unpolarized differential cross sections for the scattering of neutral gauge bosons in the nonlinear extension considered in this work. In the following, we are using $\beta_Z \equiv \sqrt{1 - 4m_Z^2/E_{\text{cm}}^2}$:

(i) $\gamma\gamma \rightarrow \gamma\gamma$

$$\frac{d\sigma}{d\Omega} = \frac{E_{\text{cm}}^6 c_\theta^8 (3 + \cos^2 \theta)^2}{4096\pi^2 \beta^4}. \quad (\text{C1})$$

(ii) $\gamma\gamma \rightarrow \gamma Z$

$$\frac{d\sigma}{d\Omega} = \frac{c_\theta^6 s_\theta^2 (E_{\text{cm}}^2 - m_Z^2)^3}{4096\pi^2 \beta^4 E_{\text{cm}}^4} [(6E_{\text{cm}}^4 - 2m_Z^4) \cos^2 \theta + 9E_{\text{cm}}^4 + (E_{\text{cm}}^2 - m_Z^2)^2 \cos^4 \theta + 2E_{\text{cm}}^2 m_Z^2 + m_Z^4]. \quad (\text{C2})$$

(iii) $\gamma\gamma \rightarrow ZZ$

$$\frac{d\sigma}{d\Omega} = \frac{c_\theta^4 s_\theta^4 E_{\text{cm}}^2 \beta_Z}{4096\pi^2 \beta^4} [9E_{\text{cm}}^4 + E_{\text{cm}}^4 \beta_Z^4 \cos^4 \theta + 6E_{\text{cm}}^4 \beta_Z^2 \cos^2 \theta - 32E_{\text{cm}}^2 m_Z^2 + 40m_Z^4]. \quad (\text{C3})$$

(iv) $\gamma Z \rightarrow \gamma\gamma$

$$\frac{d\sigma}{d\Omega} = \frac{c_\theta^6 s_\theta^2 (E_{\text{cm}}^2 - m_Z^2)}{6144\pi^2 \beta^4} [(6E_{\text{cm}}^4 - 2m_Z^4) \cos^2 \theta + 9E_{\text{cm}}^4 + (E_{\text{cm}}^2 - m_Z^2)^2 \cos^4 \theta + 2E_{\text{cm}}^2 m_Z^2 + m_Z^4]. \quad (\text{C4})$$

(v) $\gamma Z \rightarrow \gamma Z$

$$\begin{aligned} \frac{d\sigma}{d\Omega} = & \frac{c_\theta^4 s_\theta^4 (E_{\text{cm}}^2 - m_Z^2)^4}{49152\pi^2 \beta^4 E_{\text{cm}}^{10}} [99E_{\text{cm}}^8 + 20E_{\text{cm}}^6 m_Z^2 + 74E_{\text{cm}}^4 m_Z^4 + 20E_{\text{cm}}^2 m_Z^6 + (E_{\text{cm}}^2 - m_Z^2)^4 \cos 4\theta - 8m_Z^4 (E_{\text{cm}}^2 - m_Z^2)^2 \cos 3\theta \\ & - 8m_Z^4 (11E_{\text{cm}}^4 + 2E_{\text{cm}}^2 m_Z^2 + 7m_Z^4) \cos \theta + 4(7E_{\text{cm}}^8 - 4E_{\text{cm}}^6 m_Z^2 + 4E_{\text{cm}}^4 m_Z^4 - 4E_{\text{cm}}^2 m_Z^6 + 7m_Z^8) \cos 2\theta + 35m_Z^8]. \end{aligned} \quad (\text{C5})$$

(vi) $\gamma Z \rightarrow ZZ$

$$\begin{aligned} \frac{d\sigma}{d\Omega} = & \frac{c_\theta^2 s_\theta^6 \beta_Z (E_{\text{cm}}^2 - m_Z^2)}{6144\pi^2 \beta^4 E_{\text{cm}}^4} [9E_{\text{cm}}^8 - 30E_{\text{cm}}^6 m_Z^2 + 45E_{\text{cm}}^4 m_Z^4 + (E_{\text{cm}}^4 - 5E_{\text{cm}}^2 m_Z^2 + 4m_Z^4)^2 \cos^4 \theta \\ & + 2E_{\text{cm}}^4 \beta_Z^2 (3E_{\text{cm}}^4 + m_Z^4) \cos^2 \theta]. \end{aligned} \quad (\text{C6})$$

-
- [1] O. Halpern, Scattering processes produced by electrons in negative-energy states, *Phys. Rev.* **44**, 855 (1933).
[2] W. Heisenberg, Bemerkungen zur Diracschen Theorie des Positrons, *Z. Phys.* **90**, 209 (1934).
[3] M. Born and L. Infeld, Foundations of the new field theory, *Nature (London)* **132**, 1004 (1933).
[4] W. Heisenberg and H. Euler, Consequences of Dirac's theory of positrons, *Z. Phys.* **98**, 714 (1936).
[5] S. I. Kruglov, Born-Infeld-type electrostatics and magnetic black holes, *Ann. Phys. (Amsterdam)* **383**, 550 (2017).
[6] S. I. Kruglov, Dyonic black holes with nonlinear logarithmic electrostatics, *Gravitation Cosmol.* **25**, 190 (2019).
[7] N. Bretón, Nonlinear electrostatics and cosmology, *J. Phys. Conf. Ser.* **229**, 012006 (2010).
[8] R. García-Salcedo and N. Bretón, Born-infeld cosmologies, *Int. J. Mod. Phys. A* **15**, 4341 (2000).
[9] P. Gaete and J. A. Helayël-Neto, Finite field-energy and interparticle potential in logarithmic electrostatics, *Eur. Phys. J. C* **74**, 2816 (2014).
[10] P. Gaete and J. A. Helayël-Neto, Remarks on nonlinear electrostatics, *Eur. Phys. J. C* **74**, 3182 (2014).
[11] P. Gaete and J. A. Helayël-Neto, A note on nonlinear electrostatics, *Europhys. Lett.* **119**, 51001 (2017).
[12] M. J. Neves, J. B. de Oliveira, L. P. R. Ospedal, and J. A. Helayël-Neto, Dispersion relations in non-linear

- electrodynamics and the kinematics of the Compton effect in a magnetic background, *Phys. Rev. D* **104**, 015006 (2021).
- [13] I. Gullu and S. H. Mazharimousavi, Double-logarithmic nonlinear electrodynamics, *Phys. Scr.* **96**, 045217 (2021).
- [14] I. Bandos, K. Lechner, D. Sorokin, and P. K. Townsend, Nonlinear duality-invariant conformal extension of Maxwell's equations, *Phys. Rev. D* **102**, 121703(R) (2020).
- [15] ATLAS Collaboration, Evidence for light-by-light scattering in heavy-ion collisions with the ATLAS detector at the LHC, *Nat. Phys.* **13**, 852 (2017).
- [16] CMS Collaboration, Evidence for light-by-light scattering and searches for axion-like particles in ultraperipheral PbPb collisions at $\sqrt{s_{NN}} = 5.02$ TeV, *Phys. Lett. B* **797**, 134826 (2019).
- [17] ATLAS Collaboration, Observation of Light-by-Light Scattering in Ultraperipheral Pb + Pb Collisions with the ATLAS Detector, *Phys. Rev. Lett.* **123**, 052001 (2019).
- [18] P. Dirac, Quantised singularities in the electromagnetic field, *PAM Dirac Proc. Roy. Soc. Lond. A* **133**, 60 (1931).
- [19] Y. M. Cho and D. Maison, Monopoles in Weinberg-Salam model, *Phys. Lett. B* **391**, 360 (1997).
- [20] Y. M. Cho, K. Kim, and J. H. Yoon, Finite energy electroweak dyon, *Eur. Phys. J. C* **75**, 67 (2015).
- [21] J. Ellis, N. E. Mavromatos, and T. You, The price of an electroweak monopole, *Phys. Lett. B* **756**, 29 (2016).
- [22] P. Zhang, L. Zou, and Y. M. Cho, Regularization of electroweak monopole by charge screening and BPS energy bound, *Eur. Phys. J. C* **80**, 280 (2020).
- [23] S. Arunasalam and A. Kobakhidze, Electroweak monopoles and the electroweak phase transition, *Eur. Phys. J. C* **77**, 444 (2017).
- [24] P. De Fabritiis and J. A. Helayël-Neto, Electroweak monopoles with a non-linearly realized weak hypercharge, *Eur. Phys. J. C* **81**, 788 (2021).
- [25] B. Acharya *et al.* (MoEDAL Collaboration), The physics programme of the MoEDAL experiment at the LHC, *Int. J. Mod. Phys. A* **29**, 1430050 (2014).
- [26] P. Niau Akmansoy and L. G. Medeiros, Constraining Born-Infeld-like nonlinear electrodynamics using hydrogen's ionization energy, *Eur. Phys. J. C* **78**, 143 (2018).
- [27] M. Fouché, R. Battesti, and C. Rizzo, Limits on nonlinear electrodynamics, *Phys. Rev. D* **93**, 093020 (2016).
- [28] J. Ellis, N. E. Mavromatos, and T. You, Light-by-Light Scattering Constraint on Born-Infeld Theory, *Phys. Rev. Lett.* **118**, 261802 (2017).
- [29] J. Ellis and S. Ge, Constraining Gluonic Quartic Gauge Coupling Operators with $gg \rightarrow \gamma\gamma$, *Phys. Rev. Lett.* **121**, 041801 (2018).
- [30] E. S. Fradkin and A. A. Tseytlin, Non-linear electrodynamics from quantized strings, *Phys. Lett.* **163B**, 123 (1985).
- [31] C. G. Callan and J. M. Maldacena, Brane dynamics from the Born-Infeld action, *Nucl. Phys.* **B513**, 198 (1998).
- [32] M. Baillargeon and F. Boudjema, Contribution of the bosonic loops to the three photon decay of the Z, *Phys. Lett. B* **272**, 158 (1991).
- [33] X. Pham, Non-Abelian effects in nonlinear quantum electrodynamics and in Z0 decay into three photons, *Phys. Lett. B* **272**, 373 (1991).
- [34] E. W. N. Glover and A. G. Morgan, Z boson decay into photons, *Z. Phys. C* **60**, 175 (1993).
- [35] P. A. Zyla *et al.* (Particle Data Group), Review of particle physics, *Prog. Theor. Exp. Phys.* **2020**, 083C01 (2020) and 2021 update.
- [36] ATLAS Collaboration, Search for new phenomena in events with at least three photons collected in pp collisions at $\sqrt{s} = 8$ TeV with the ATLAS detector, *Eur. Phys. J. C* **76**, 210 (2016).
- [37] L3 Collaboration, Search for anomalous $Z \rightarrow \gamma\gamma\gamma$ events at LEP, *Phys. Lett. B* **345**, 609 (1995).
- [38] S. Villa, Gauge boson couplings at LEP, *Nucl. Phys.* **B142**, 391 (2005).
- [39] M. A. Perez, G. Tavares-Velasco, and J. J. Toscano, New physics effects in rare Z decays, *Int. J. Mod. Phys. A* **19**, 159 (2004).
- [40] M. Stohr and J. Horejsi, Effective lagrangians for the Z boson decay into photons, *Phys. Rev. D* **49**, 3775 (1994).
- [41] M. J. Neves, L. P. R. Ospedal, J. A. Helayël-Neto, and Patricio Gaete, Considerations on anomalous photon and Z-boson self-couplings from the Born-Infeld weak hypercharge action, [arXiv:2109.11004](https://arxiv.org/abs/2109.11004).
- [42] K. Buesser, The international linear collider, [arXiv:1306.3126](https://arxiv.org/abs/1306.3126).
- [43] D. M. Asner *et al.*, ILC Higgs white paper, [arXiv:1310.0763v4](https://arxiv.org/abs/1310.0763v4).
- [44] K. Fujii *et al.*, ILC study questions for snowmass 2021, [arXiv:2007.03650v3](https://arxiv.org/abs/2007.03650v3).
- [45] K. Fujii *et al.*, Tests of the standard model at the international linear collider, [arXiv:1908.11299](https://arxiv.org/abs/1908.11299).
- [46] A. Blondel and P. Janot, FCC-ee overview: New opportunities create new challenges, [arXiv:2106.13885](https://arxiv.org/abs/2106.13885).
- [47] P. Azzurri, G. Bernardi, S. Braibant, D. d'Enterria, J. Eysermans, P. Janot, A. Li, and E. Perez, A special Higgs challenge: Measuring the mass and production cross section with ultimate precision at FCC-ee, *Eur. Phys. J. Plus* **137**, 23 (2021).
- [48] W. de Boer, Precision experiments at LEP, *Adv. Ser. Dir. High Energy Phys.* **23**, 107 (2015).
- [49] T. Lesiak Future e^+e^- colliders at the energy frontier, *EPJ Web Conf.* **206**, 08001 (2019).
- [50] CEPC-SPPC Study Group, Electroweak physics at CEPC, *Proc. Sci. ICHEP2016* (2016) 692.
- [51] The Compact Linear Collider (CLIC)—Project Implementation Plan, edited by M. Aicheler *et al.* (Report No. CERN-2018-010-M, 2018).
- [52] L3 Collaboration, A test of electrodynamics in the reaction $e^+e^- \rightarrow \gamma\gamma(\gamma)$, *Phys. Lett. B* **288**, 404 (1992).
- [53] L3 Collaboration, Study of multiphoton final states and tests of QED in e^+e^- collisions at \sqrt{s} up to 209 GeV, *Phys. Lett. B* **531**, 28 (2002).
- [54] A. F. Zarnecki, On the physics potential of ILC and CLIC, *Proc. Sci., CORFU2019* (2020) 037 [[arXiv:2004.14628](https://arxiv.org/abs/2004.14628)].
- [55] F. A. Berends and R. Kleiss, Distributions for electron-positron annihilation into two and three photons, *Nucl. Phys.* **B186**, 22 (1981).
- [56] S. Yellin, $\gamma\gamma$ physics with virtual bremsstrahlung, *Int. J. Mod. Phys. A* **11**, 1645 (1996).
- [57] Kwang-Je Kim, Gamma gamma collider based on Compton back scattering, *Nucl. Instrum. Methods Phys. Res., Sect. A* **393**, 530 (1997).
- [58] C. Friberg, $\gamma\gamma$ physics at linear colliders, [arXiv:hep-ph/9911444](https://arxiv.org/abs/hep-ph/9911444).

- [59] B. Badelek *et al.*, TESLA technical design report, Part VI, Chapter 1: The photon collider at TESLA, *Int. J. Mod. Phys. A* **19**, 5097 (2004).
- [60] R. Appleby and P. Bambade, Photon production at the interaction point of the ILC, [arXiv:0803.3519](https://arxiv.org/abs/0803.3519).
- [61] H. Burkhardt, Multi-TeV CLIC photon collider option, *Nucl. Instrum. Methods Phys. Res., Sect. A* **472**, 67 (2001).
- [62] I.F. Ginzburg and G.L. Kotkin, High energy photon collider, [arXiv:1910.13961](https://arxiv.org/abs/1910.13961).
- [63] V.I. Telnov, Principles of photon colliders, *Nucl. Instrum. Methods Phys. Res., Sect. A* **355**, 3 (1995).
- [64] A. Denner, S. Dittmaier, and R. Schuster, Radiative corrections to $\gamma\gamma \rightarrow W^+W^-$ in the electroweak Standard Model, *Nucl. Phys.* **B452**, 80 (1995).
- [65] E. Yehudai, Probing W gamma couplings using $\gamma\gamma \rightarrow W^+W^-$, *Phys. Rev. D* **44**, 3434 (1991).
- [66] F.-X. Dong and X.-J. Zhou, $\gamma\gamma \rightarrow \gamma Z$ scattering and its related processes, *Mod. Phys. Lett. A* **15**, 2387 (2000).
- [67] D. A. Dicus and C. Kao, Production of Z boson pairs at photon linear colliders, *Phys. Rev. D* **49**, 1265 (1994).
- [68] G. V. Jikia, Z boson pair production in high energy photon-photon collisions and the Higgs signal, *Phys. Lett. B* **298**, 224 (1993).
- [69] R. Karplus and M. Neuman, The scattering of light by light, *Phys. Rev.* **83**, 776 (1951).
- [70] L. Meitner and H. Kötters, Ueber die streuung kurzweiliger γ -strahlen, *Z. Phys.* **84**, 137 (1933).
- [71] B. De Tollis, The scattering of photons by photons, *Nuovo Cimento* **35**, 1182 (1965).
- [72] D. d'Enterria and G. G. Silveira, Observing Light-by-Light Scattering at the Large Hadron Collider, *Phys. Rev. Lett.* **111**, 080405 (2013); **116**, 129901(E) (2016).
- [73] C. Baldenegro, S. Fichet, G. von Gersdorff, and C. Royon, Probing the anomalous $\gamma\gamma Z$ coupling at the LHC with proton tagging, *J. High Energy Phys.* **06** (2017) 142.
- [74] S.C. Inan and A.V. Kisselev, Probing anomalous $\gamma\gamma Z$ couplings through γZ production in $\gamma\gamma$ collisions at the CLIC, *J. High Energy Phys.* **10** (2021) 121.
- [75] S. Fichet, G. von Gersdorff, O. Kepka, B. Lenzi, C. Royon, and M. Saimpert, Probing new physics in diphoton production with proton tagging at the Large Hadron Collider, *F* **89**, 114004 (2014).
- [76] S. Fichet, G. von Gersdorff, B. Lenzi, C. Royon, and M. Saimpert, Light-by-light scattering with intact protons at the LHC: From standard model to new physics, *J. High Energy Phys.* **02** (2015) 165.
- [77] S.C. Inan and A.V. Kisselev, Probing anomalous quartic $\gamma\gamma\gamma\gamma$ couplings in light-by-light collisions at the CLIC, *Eur. Phys. J. C* **81**, 664 (2021).
- [78] M. Köksal, V. Ari, and A. Senol, Search for anomalous quartic $ZZ\gamma\gamma$ couplings in photon-photon collisions, *Adv. High Energy Phys.* **2016**, 8672391 (2016).
- [79] E. Gurkanli, V. Ari, M. Köksal, A. Gutiérrez-Rodríguez, and M. A. Hernández-Ruiz, Study of the projected sensitivity on the anomalous quartic gauge couplings via $Z\gamma\gamma$ production at the CLIC, [arXiv:2112.03948](https://arxiv.org/abs/2112.03948).
- [80] O. J. P. Eboli, M. C. Gonzalez-Garcia, and J. K. Mizukoshi, $pp \rightarrow jje^\pm\mu^\pm\nu\nu$ and $jje^\pm\mu^\mp\nu\nu$ at $\mathcal{O}(\alpha_{\text{em}}^6)$ and $\mathcal{O}(\alpha_{\text{em}}^4\alpha_s^2)$ for the study of the quartic electroweak gauge boson vertex at CERN LHC, *Phys. Rev. D* **74**, 073005 (2006).
- [81] CMS Collaboration, Measurement of the cross section for electroweak production of a Z boson, a photon and two jets in proton-proton collisions at $\sqrt{s} = 13$ TeV and constraints on anomalous quartic couplings, *J. High Energy Phys.* **06** (2020) 076.
- [82] CMS Collaboration, Evidence for electroweak production of four charged leptons and two jets in proton-proton collisions at $\sqrt{s} = 13$ TeV, *Phys. Lett. B* **812**, 135992 (2021).
- [83] CMS Collaboration, Measurements of the $pp \rightarrow W^\pm\gamma\gamma$ and $pp \rightarrow Z\gamma\gamma$ cross sections at $\sqrt{s} = 13$ TeV and limits on anomalous quartic gauge couplings, *J. High Energy Phys.* **10** (2021) 174.
- [84] CMS Collaboration, Measurement of the electroweak production of $Z\gamma$ and two jets in proton-proton collisions at $\sqrt{s} = 13$ TeV and constraints on anomalous quartic gauge couplings, *Phys. Rev. D* **104**, 072001 (2021).
- [85] The CMS and TOTEM Collaborations, First search for exclusive diphoton production at high mass with tagged protons in proton-proton collisions at $\sqrt{s} = 13$ TeV, [arXiv:2110.05916](https://arxiv.org/abs/2110.05916).
- [86] J. Ellis, S. Ge, and K. Ma, Hadron collider probes of the quartic couplings of gluons to the photon and Z bosons, [arXiv:2112.06729](https://arxiv.org/abs/2112.06729).